

Performance and design of reinforced slopes considering regional hydrological conditions

K-H Yang¹, T. S. Nguyen², Y-H Li³ and B. Leshchinsky⁴

¹Associate Professor, Department of Civil Engineering, National Taiwan University (NTU), 1, Sec. 4, Roosevelt Rd., Taipei 106, Taiwan, E-mail: khyang@ntu.edu.tw (corresponding author)

²PhD candidate, Department of Civil and Construction Engineering, National Taiwan University of Science and Technology (Taiwan Tech), 43, Sec. 4, Keelung Rd., Taipei 106, Taiwan, E-mail: sonnt@nuce.edu.vn

³Research Assistant, Department of Civil and Construction Engineering, National Taiwan University of Science and Technology (Taiwan Tech), 43, Sec. 4, Keelung Rd., Taipei 106, Taiwan, E-mail: rm325896@gmail.com

⁴Associate Professor and Richardson Chair, Department of Forest Engineering, Resources and Management, Oregon State University, Corvallis, OR, USA, E-mail: ben.leshchinsky@oregonstate.edu

Received 30 November 2018, revised 26 March 2019, accepted 23 May 2019, published 14 August 2019

ABSTRACT: This study presents a series of numerical analyses investigating the impact of rainfall on the performance and design of geosynthetic-reinforced soil slopes (RSSs). The importance of considering regional hydrological conditions for designs of RSSs, particularly when marginal soil is used as backfill, is demonstrated and highlighted. RSSs with backfills containing five different fines contents subjected to various combinations of initial hydraulic conditions and major rainfall events were modeled. The input rainfall was determined from the rainfall intensity–duration–frequency (I–D–F) curves to realistically account for the impact of regional hydrological conditions. The hydraulic responses and stability of the RSSs including their porewater pressure development and factor of safety were then evaluated and compared. The results revealed that the applied rainfall scenarios had little influence on the performance of RSSs with high-quality backfills (i.e. backfill with low fines content), whereas those with prolonged rainfall duration substantially affected the performance of RSSs with high fines content backfills. Rainfall thresholds were established for the RSSs with various backfills and initial conditions and compared with the regional I–D–F curves to provide a simplified and robust method for facilitating backfill selection and assessing the failure risk of RSSs.

KEYWORDS: Geosynthetics, Geosynthetic-reinforced soil, Marginal backfill, Rainfall threshold, Intensity–duration–frequency curve

REFERENCE: Yang, K-H, Nguyen, T. S., Li, Y-H and Leshchinsky, B. (2019). Performance and design of reinforced slopes considering regional hydrological conditions. *Geosynthetics International*, 26, No. 5, 451–473. [https://doi.org/10.1680/jgein.19.00031]

1. INTRODUCTION

The design methodologies for mechanically stabilized earth (MSE) and geosynthetic-reinforced soil (GRS) structures have been developed for decades and are widely used in practice (Elias *et al.* 2001; AASHTO 2002; Berg *et al.* 2009; NCMA 2010); however, failures of these structures have still often been reported in the literature. Berg (2010) reported that these structures have a significant failure rate of approximately 5%. Koerner and Koerner (2013, 2018) investigated 320 failure cases of GRS structures that experienced excessive deformation or collapse. The statistical data from these GRS structures revealed that 73% of the failure cases had used silt or clay as backfill in the reinforced zone, 63% were caused by

internal or external water, and 99% were due to improper design or construction. Wu and Chou (2013) examined 19 failure cases of GRS structures in Taiwan and reported that intense rainfall, inadequate project planning and site exploration, and poor construction quality were the key reasons for the observed failures. Valentine (2013) assessed the factors that contribute to the poor performance of GRS structures and reported similar findings from failure analyses.

Case studies have been conducted to investigate the failure mechanisms and factors triggering failure of reinforced structures (Leonards *et al.* 1994; Mitchell and Zornberg 1995; Scarborough 2005; Yoo and Jung 2006; Shibuya *et al.* 2007; Wu and Tang 2008; Hossain *et al.* 2012; Liu *et al.* 2012; Kim and Borden 2013; Miyata and

Table 1. Summary of failure case histories of reinforced structures triggered by rainfall

Reference	Location	Reinforced structure			Backfill				Rainfall event	
		Type	Height, <i>H</i> (m)	Failure mode	Soil type (classification)	Fines content, FC (%)	Cohesion ^a , <i>c'</i> or <i>c</i> (kPa)	Friction angle ^a , ϕ' or ϕ (°)	Accumulated rainfall, <i>R</i> (mm)	Duration, <i>D</i> (h)
Kim and Borden (2013)	North Carolina, USA	Wall	5.4	Localized collapse	Low plasticity clay (CL)	58	0–3	26–30	N/A	A few months
Miyata and Shinoda (2016)	Japan	Wall	10.7	Internal	Cohesive soil	N/A	14.7	34.7	N/A	N/A
Yoo and Jung (2006)	Chungnam, Korea	Wall	12.5	Compound	Clayey sand (SC)	30	13	22	780	1464
Liu <i>et al.</i> (2012)	Nantou, Taiwan	Slope	40	Compound	Laterite gravel with clay	42	54	28	503	24
Yang <i>et al.</i> (2019)	Taichung, Taiwan	Slope	26	Compound	Silty clay (CL-ML)	60	6.3	37	750	264
Leonards <i>et al.</i> (1994)	Kentucky, USA	Wall	6.4	Deep-seated	Silty clay/clayey silt	N/A	0.15	25.7	119	240
Shibuya <i>et al.</i> (2007)	Yabu, Japan	Wall	23	Deep-seated	Cement-mixed silty clay	40	46.3	7.77	237	23

^aShibuya *et al.* (2007) provides total shear strength parameters and other references provide effective parameters; N/A: information is not available.

Shinoda 2016; Yang *et al.* 2019). Table 1 summarizes detailed information (wall geometry, failure mode, backfill type, and rainfall) for selected failure case histories of GRS structures compiled from the literature. These studies concluded that intense and prolonged rainfall, use of marginal backfill containing a certain amount of fines (typically with low permeability), and insufficient and malfunctioning drainage systems were the primary causes of GRS structure failure.

Many experimental and numerical studies have been conducted to evaluate the performance and failure mechanism of GRS structures under rainfall or seepage conditions (Iryo and Rowe 2005; Chen *et al.* 2007; Garcia *et al.* 2007; Raisinghani and Viswanadham 2011; Portelinha *et al.* 2013; Portelinha and Zornberg 2014; Bhattacharjee and Viswanadham 2015; Thuo *et al.* 2015; Balakrishnan and Viswanadham 2016; Vahedifard *et al.* 2016; Portelinha and Zornberg 2017; Van *et al.* 2017; Viswanadham *et al.* 2017; Yang *et al.* 2018). These studies applied hypothetical rainfall (by assuming an arbitrary rainfall intensity and duration) to GRS structures and found that the rainfall had an adverse impact on the performance of GRS structures, especially for those backfilled with marginal soils. The stability of GRS structures substantially decreases upon rainfall infiltration because of the loss of matric suction as the wetting front advances and the development of positive porewater pressure (PWP) as the phreatic level rises (Figure 1). Vahedifard *et al.* (2017) quantitatively assessed the resilience of GRS walls with marginal backfill under extreme precipitation events. The regional hydrological data, determined from the rainfall intensity–duration–frequency (I–D–F) curves for the Seattle region, were used as input rainfall in their study. The results of their study indicated that the impact on GRS walls can be significant when extreme precipitation events occur.

Based on the aforementioned studies, the design of GRS structures against rainfall is an important and urgent task considering the increasing interest in using marginal soils as backfill owing to both economic and environmental considerations. Specifically, effective means of incorporating the potential effects of rainfall into designs remains challenging because it involves complex interactions and mutual influence among hydrological, geological, and geotechnical parameters. According to conventional practice in Taiwan, the effect of rainfall on a slope is typically modeled by raising the phreatic surface level in the slope stability analysis according to groundwater monitoring data recorded over at least one rainy season. However, this approach is seldom applicable to fill-type retaining structures such as GRS structures because no groundwater monitoring data within the retaining structure are available before these structures are built. Consequently, the location of the phreatic surface within a GRS structure upon rainfall must be assumed, which can lead to conservative or hazardous designs, depending on the hydraulic response of GRS structures to the site-specific potential rainfall. In addition, assuming the phreatic level means that a design does not consider the influence of soil permeability, drainage systems, and local rainfall conditions, which may discourage an

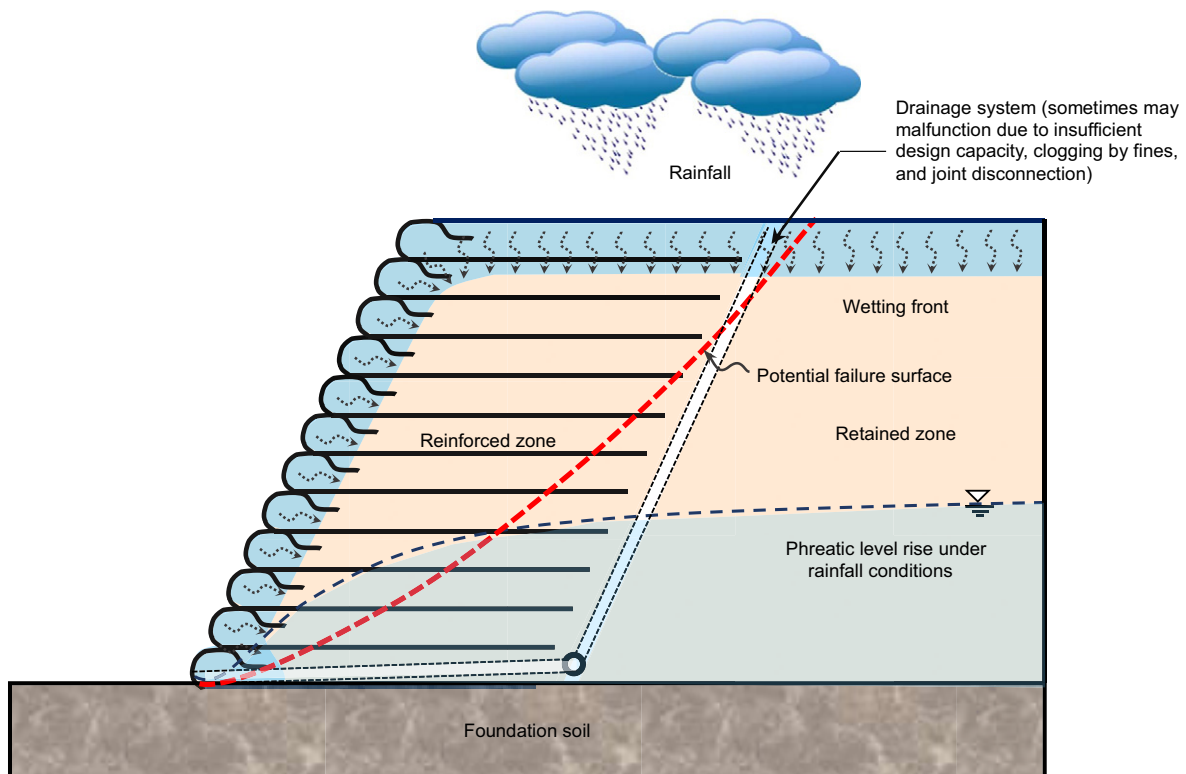


Figure 1. Conceptual illustration of rainfall-induced water infiltration and phreatic level rise in a GRS structure

innovative or tailored design-specific project. Therefore, robust design methods must be adopted that couple hydrological and geotechnical parameters to obtain the optimal design for each site-specific condition.

Determination of critical rainfall that triggers slope failure (i.e. the rainfall threshold) is one of the most common approaches to providing a quick and easy assessment of landslide risk for establishing early warning systems for rainfall-induced landslides (Terlien 1998). The rainfall threshold, mostly represented as the relationship between rainfall intensity and the duration of the rainfall event (namely the intensity–duration thresholds), was first proposed by Caine (1980) and has been applied in many other studies (Aleotti 2004; Guzzetti *et al.* 2007; Matsushi and Matsukura 2007; Saito *et al.* 2010; Chen *et al.* 2015; Chinkulkijniwat *et al.* 2016; Robinson *et al.* 2016; Suradi *et al.* 2016; Hong *et al.* 2018). The rainfall threshold has been proposed on both empirical and physical bases: empirical thresholds are defined by collecting and analyzing rainfall data at the onset of landslide events, whereas physical thresholds are based on numerical models that consider the relationships among rainfall, porewater pressure, and slope stability (Aleotti 2004). Notably, most research has focused on establishing rainfall thresholds for natural (or unreinforced) slopes, but, to date, little attention has been paid to establishing rainfall thresholds for reinforced slopes.

The present study investigated the impact of rainfall on the performance and design of geosynthetic-reinforced soil slopes (RSS). In order to realistically account for the regional hydrological conditions, the rainfall I–D–F curve of Taipei, Taiwan, was used as an example to determine the input rainfall. The numerical analyses, including

transient seepage and slope stability analyses, were performed using SEEP/W and SLOPE/W software (Geo-Slope 2012a, 2012b), respectively, to calculate the variations of PWP and factor of safety (FS) of RSSs during rainfall. A framework of unsaturated soil mechanics was incorporated into the simulations to model the hydraulic and mechanical responses of RSSs when soil transforms from an unsaturated to a saturated condition upon infiltration of rainfall.

The main objectives of the present study are to (1) evaluate the hydraulic responses and stability of RSSs with various backfills under different rainfall scenarios; (2) assess improved design methods for RSSs against rainfall; (3) establish rainfall thresholds for RSSs considering various backfills and initial conditions; (4) assess the failure risk of RSSs under regional potential rainfall by comparing the rainfall thresholds for RSSs with the regional I–D–F curve. This study integrates geotechnical engineering with hydrology to quantify how regional hydrological conditions may affect the performance and design of GRS structures. The results of this study provide insightful information regarding backfill selection, stability evaluation and improved design recommendations for GRS structures to guard against the potentially negative effects of rainfall.

2. MODEL VALIDATION

2.1. Numerical simulation of a failure case

A numerical model was first validated using the failure case history of a GRS wall in Korea reported by Yoo and Jung (2006). The investigated case was a 7.4-m-high wall

backfilled with completely decomposed granite soil with a fines content of approximately 30%. The GRS wall collapsed in late July 2003 due to heavy and prolonged rainfall during the monsoon season. The failure mode was identified as a compound failure in which the failure surface partially cut through the reinforced zone and partially passed through the retained zone.

Table 1 provides detailed information of the failure case. The soil–water characteristic curve (SWCC) and hydraulic conductivity function (k -function) reported by Yoo and Jung (2006) were adopted in the transient seepage analysis to calculate the variation of PWP during rainfall. The input saturated hydraulic conductivity value was $k_{\text{sat}} = 5 \times 10^{-7}$ m/s, measured from falling head permeability tests as reported by Yoo and Jung (2006).

The unsaturated soil shear strength function proposed by Vanapalli *et al.* (1996) was used in the slope stability analysis to determine FS.

$$\tau = c' + (\sigma_n - u_a) \tan \phi' + \left(\frac{\theta_w - \theta_r}{\theta_s - \theta_r} \right) [(u_a - u_w) \tan \phi^r] \quad (1)$$

where τ is the soil shear strength; c' is the effective cohesion; ϕ' is the effective friction angle; $(\sigma_n - u_a)$ is the net normal stress (σ_n and u_a are the total normal stress and pore-air pressure acting on the failure plane, respectively); θ_w is the volumetric water content; θ_s is the saturated volumetric water content; θ_r is the residual volumetric water content; $(u_a - u_w)$ is the matric suction (where u_w is the porewater pressure). The input parameters $\theta_s = 0.4$ and $\theta_r = 0.04$ were deduced from the provided SWCC, and $c' = 13$ kPa and $\phi' = 22^\circ$ were determined from consolidated undrained triaxial tests as reported by Yoo and Jung (2006). Notably, Yoo and Jung's study used Fredlund's shear strength function for unsaturated soils (Fredlund *et al.* 1978).

$$\tau = c' + (\sigma_n - u_a) \tan \phi' + (u_a - u_w) \tan \phi^b \quad (2)$$

where ϕ^b is the angle indicating the rate of increase in shear strength relative to the matric suction; the rest of the parameters have been defined earlier. As has been well recognized, the unsaturated soil shear strength and matric suction exist in a nonlinear relationship (Vanapalli *et al.* 1996; Rassam and Cook 2002; Zhang *et al.* 2014). Fredlund's function is a linear form of the extended Mohr-Coulomb shear strength equation that cannot accurately model the nonlinear relationship of unsaturated soil. In addition, Fredlund's function requires an assumption of a constant value for the parameter ϕ^b to quantify the rate of increase in shear strength relative to matric suction. By contrast, Vanapalli's function used in model validation is a nonlinear form that can better describe the nonlinear relationship between soil strength and matric suction (Vanapalli *et al.* 1996; Rassam and Cook 2002; Zhang *et al.* 2014).

Figure 2a shows the numerical model and hydraulic boundaries of the investigated GRS wall. The groundwater level, defined as the total head boundaries, was initially located 5 m below the base of the GRS wall, and it was later allowed to vary during the simulation of

rainfall infiltration. The finite element mesh consisted of 5583 triangular elements. Adaptive time stepping between 1 and 300 s was adopted to prevent numerical oscillations and enhance computational stability and accuracy (Karthikeyan *et al.* 2001; Tan *et al.* 2004).

In the transient seepage analysis, a series of inflow fluxes was first prescribed on the surface boundaries ab and cd, which conformed to the intensity and duration suggested by Yoo and Jung (2006). A small unit flux ($q = 4.5 \times 10^{-9}$ m/s) was prescribed to generate initial PWP in the range of -40 to -60 kPa in the reinforced and retained zones, corresponding to the typical matric suction values of similar fill slopes in Korea. Figure 2b shows the results of the initial PWP profiles at various cross sections, which match the measured field suction values (i.e. -40 to -60 kPa) reported by Yoo and Jung (2006). Upon generation of the initial condition, a unit flux of $q = 5.0 \times 10^{-8}$ m/s was then input on the surface boundary for 2 months (from April to May) to simulate the antecedent rainfall. Afterward, $q = 7.2 \times 10^{-8}$ m/s over the next 30 days (in June) and $q = 3.3 \times 10^{-7}$ m/s for the next 20 days (1–20 July) were prescribed on the surface boundaries to simulate the recorded rainfall in June and July. After the rainfall stopped, a zero unit flux ($q = 0$ m/s) was assigned for 10 more days (21–30 July) to simulate the post-rainfall condition. The input rainfall intensities in June and July were indicated in Figure 3.

In the slope stability analysis, the aforementioned PWP's predicted in the transient seepage analysis were applied to calculate the soil effective stress. An allowable long-term strength of 20 kN/m was input as the reinforcement tensile load, as suggested by Yoo and Jung (2006). The limit equilibrium calculations were performed using Spencer's method (Spencer 1967), which rigorously satisfies all equilibrium conditions, to evaluate the FS of the GRS structures at each rainfall stage. The circular failure surface with an optimization function, as coded in the SLOPE/W software, was specified to search for the location of the critical failure surfaces. The optimization process was automatic, starting by first dividing the circular failure surface into a number of piecewise line segments. The end points of the line segments were then adjusted until the lowest safety factor was found. More detailed explanation of the optimization process can be found in the SLOPE/W manual (Geo-Slope 2012b).

2.2. Results and comparison

Figure 3 shows the variation of FS with time. The FS gradually decreased with time and failure occurred (FS = 1) a few days before the end of rainfall. The numerical results reveal that the instability of the GRS wall was attributable to an increase in PWP (or loss of matric suction) within the reinforced and retained soils during heavy July rainfall. The estimated timing of failure was in good agreement with the observed timing. The FS calculated by Yoo and Jung (2006) was also plotted in Figure 3 to evaluate the effect of different unsaturated soil shear strength functions on the FS prediction. Compared with the FS calculated using Fredlund's function in Yoo and Jung (2006), the FS calculated using Vanapalli's

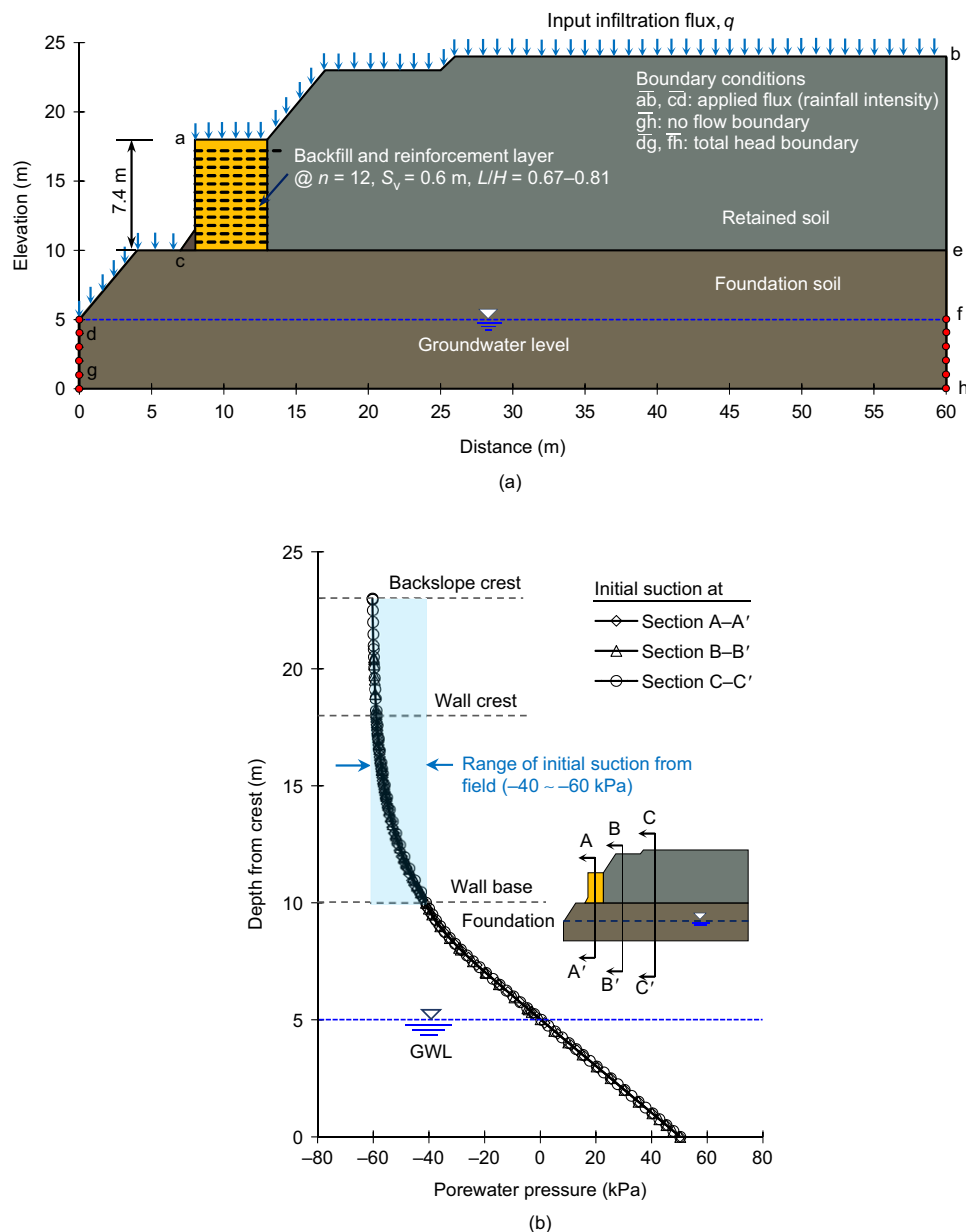


Figure 2. The GRS wall failure case for model validation: (a) numerical model and boundary conditions; (b) initial porewater pressure

in-model validation was initially lower because the non-linear form of Vanapalli's function predicts a low soil shear strength at an initially high matric suction. The FS calculated using Fredlund's and Vanapalli's functions gradually converged as rainfall continued and eventually reached $FS=1$, indicating that the predicted failure timing in this case is independent of the unsaturated soil shear strength functions used because the influence of matric suction on soil shear strength becomes minor when the wall is almost fully saturated at the point of failure.

Figure 4 shows a comparison of the predicted and observed failure surface locations. The plastic zone obtained from the coupled hydro-mechanical finite element analysis by Yoo and Jung (2006) is also provided for comparison. All of the presented failure surfaces are in good agreement. The observed compound failure mode is appropriately predicted by the numerical approach used in this study. In addition, the selection of Fredlund's or Vanapalli's functions for

unsaturated soil shear strength seems to have an insignificant influence on the predicted location of the critical failure surface.

In summary, reasonably good agreement was achieved between the observed and predicted results (i.e. failure timing and location of the critical failure surface). The results of model validation demonstrate that the numerical analysis used in this study based on the framework of unsaturated soil mechanics was appropriate for evaluating the performance of GRS structures under rainfall infiltration.

3. NUMERICAL ANALYSES

3.1. Numerical model and boundary conditions

After the numerical model was validated, a series of numerical analyses were conducted to evaluate the

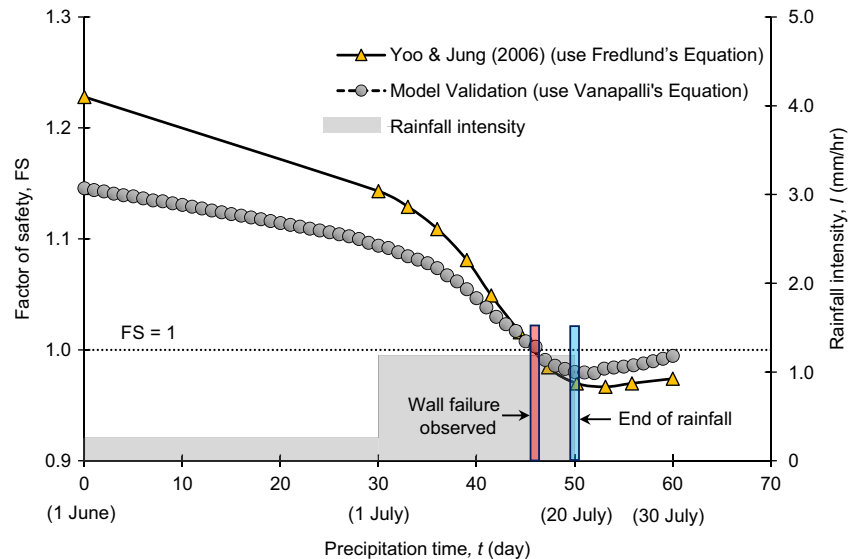


Figure 3. Model validation by comparing the observed and predicted failure timings

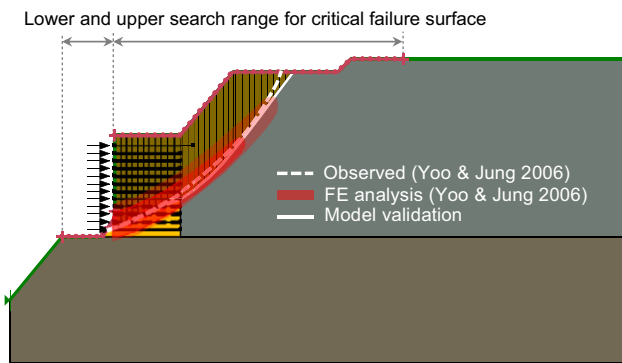


Figure 4. Model validation by comparing the observed and predicted locations of failure surfaces

performance of RSSs with various backfills under different rainfall scenarios. Figure 5 presents the numerical model of the RSS considered in this study, comprising a total of 7225 nodes and 14120 triangular elements. The mesh density was determined based on the results of a mesh sensitivity analysis to ensure the selected mesh provided reliable, accurate, and consistent results. The slope was 6.5 m high with an inclination angle of 1 H:2 V (= 63.4°). The base of the slope was 11 m long, covering both the reinforced and retained zones. Eleven layers of reinforcements were placed with a vertical spacing of 0.6 m, a typical spacing for RSSs (Elias *et al.* 2001; AASHTO 2002; Berg *et al.* 2009). The reinforcement length was $L=4.55$ m, equal to 0.7 times the slope height. The soils in the reinforced and retained zones were assumed to have the same properties. It is because many areas had no granular backfill readily available nearby, the construction used locally available soils (i.e. soils near the construction site) as alternative backfills in the practical construction of GRS structures to minimize transportation cost and environmental impact. Moreover, the locally available soils were adopted to adhere to the local regulation that specifies that the excavated and backfilled soils at the construction site should be balanced.

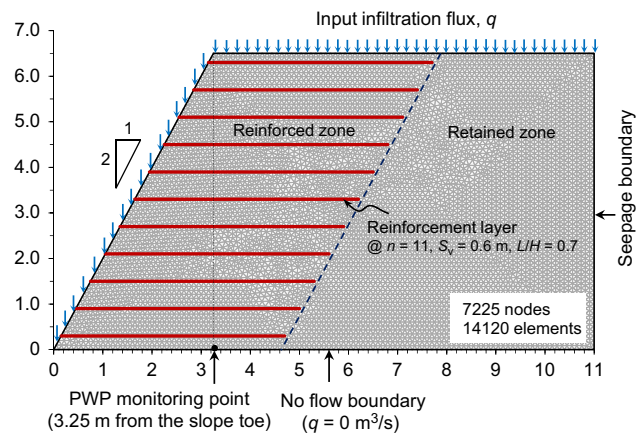


Figure 5. Numerical model of a geosynthetic-reinforced slope

For the aforementioned reasons, the same soil material is often used for both reinforced and retained zones.

The drainage system plays an important role in the performance of GRS structures. If the drainage system functions properly, it is effective in decreasing the pore-water pressure in the RSS during and after rain, increasing its stability. However, although a drainage system is typically designed and installed in the GRS structures, it could still malfunction and become ineffective with time if it is not designed and constructed carefully. Several failure case studies (Yoo and Jung 2006; Liu *et al.* 2012; Yang *et al.* 2019) reported that the drainage system had malfunctioned for reasons of insufficient design capacity, clogging by fines, or disconnection of the drainage joint. Consequently, the drainage system was not modeled in this study to account for the aforementioned problems in the drainage system.

The groundwater level was initially assumed at the bottom of the slope under normal conditions (before rainfall), which is a typical ground hydrological condition for RSSs construction sites. During the simulation of rainfall infiltration, the increase of phreatic level in the

slope was allowed by controlling the hydraulic boundary conditions at the top, side, and bottom of the slope. An inflow flux was prescribed on the top and facing surfaces of the RSS to model rainfall infiltration. A non-ponding boundary condition was specified on the slope surface to avoid excessive accumulation of rainfall. To allow seepage flowing out of the slope (i.e. free drainage surfaces), once PWP became positive at any node on the slope facing surfaces, the boundary condition was switched from the flux-specified boundary condition to a pressure-head-specified boundary condition ($h_p = 0$ m). A closed boundary was applied to the base of the RSS model, allowing the influence of the build-up of a positive PWP from the bottom of the slope to be examined. The seepage boundary was defined at the right boundary of the model to enable variations in the phreatic level during the simulation of rainfall infiltration.

3.2. Soil properties

Five backfills, FC-0, FC-6, FC-19, FC-30, and FC-60, representing soil with fines content of 0%, 6%, 19%, 30%, and 60%, respectively, were considered in the simulation. The grain size distribution curves (Figure 6), soil classification, soil unit weights, shear strength properties (Table 2), and saturated hydraulic conductivities (Table 3) of all backfills were directly adopted from several studies on GRS structures (Yoo and Jung 2006; Miyata *et al.* 2010; Portelinha *et al.* 2013; Yang *et al.* 2018). Figure 6 also shows the zones of compliant and marginal soils recommended in design guidelines (Elias *et al.* 2001; Berg *et al.* 2009; NCMA 2010) for comparison. It is observed

that the grain size distribution curves of FC-19, FC-30, and FC-60 mainly fell within the gradations defined as marginal soil.

The interface efficiency factor in Table 2 is used to calculate the soil–geogrid interface shear strength parameters (c'_a and δ') and is expressed as follows

$$E_{inter} = \frac{c'_a}{c'} = \frac{\tan \delta'}{\tan \phi'} \quad (3)$$

where E_{inter} is the interface efficiency factor; c'_a and c' are the interface and soil cohesion, δ' and ϕ' are the interface and soil friction angle, respectively. The E_{inter} values were assumed on the basis of experimental studies on the soil–geogrid interface (Eigenbrod and Locker 1987; Koutsourais *et al.* 1998; Abu-Farsakh *et al.* 2007; Liu *et al.* 2009; Esmaili *et al.* 2014; Choudhary and Krishna 2016). As shown in Table 2, the E_{inter} value decreases as the fines content increases. The soil–geogrid interface shear strength was used to calculate the part of reinforcement tensile load governed by the pullout resistance, as discussed later in this section.

The soil hydraulic characteristic data (i.e. SWCCs and k -functions) of FC-30 and FC-60, provided by Yoo and Jung (2006) and Yang *et al.* (2019), respectively, were directly adopted for the simulations in this study. Because the hydraulic characteristic data of FC-0, FC-6, and FC-19 are not available in the original references (Miyata *et al.* 2010; Portelinha *et al.* 2013), the SWCCs and k -functions of these backfills were estimated by following procedures. First, the SWCCs of FC-0, FC-6, and FC-19 were estimated using the predictive method presented by Zapata *et al.* (2000), which is based on the grain size distribution and index properties of soil. After the SWCCs of these backfills were obtained, the van Genuchten–Mualem model (Mualem 1976; van Genuchten 1980) was used to determine the fitting parameter α and n values of the SWCCs (Equation 4). Last, the van Genuchten–Mualem model with the determined fitting parameter values was applied to predict the k -functions of these backfills (Equation 5).

$$\theta_w = \theta_r + (\theta_s - \theta_r) [1 + \{\alpha(u_a - u_w)\}^n]^{-(1/n)-1} \quad (4)$$

$$k = k_{sat} \frac{[1 - \{\alpha(u_a - u_w)\}^{(n-1)}] [1 + \{\alpha(u_a - u_w)\}^n]^{n_1((1/n)-1)}^2}{[1 + \{\alpha(u_a - u_w)\}^n]^{(1/2)-(1/2n)}} \quad (5)$$

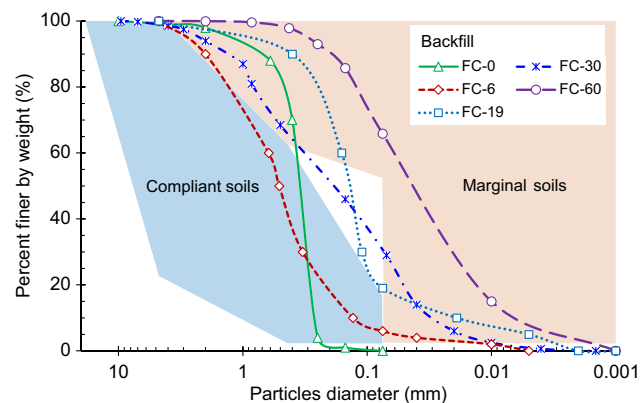


Figure 6. Grain size distribution curves of various backfills used in this study and zones of compliant and marginal soils recommended in design guidelines

where α and n are the curve fitting parameters of the van Genuchten–Mualem model, representing the air-entry

Table 2. Soil and soil-geogrid interface properties for backfills used in this study

Backfill	Reference	Soil classification	Fines content, FC (%)	Unit weight, γ (kN/m ³)	Effective cohesion, c' (kPa)	Effective friction angle, ϕ' (°)	Interface efficiency factor E_{inter}
FC-0	Portelinha <i>et al.</i> (2013)	Sand (SP)	0	16.7	0	40	0.9
FC-6	Miyata <i>et al.</i> (2010)	Sand (SP)	6	16.0	0	36	0.8
FC-19	Miyata <i>et al.</i> (2010)	Silty sand (SM)	19	15.4	2	30	0.7
FC-30	Yoo and Jung (2006)	Clayey sand (SC)	30	19.0	13	22	0.6
FC-60	Yang <i>et al.</i> (2019)	Silty clay (CL-ML)	60	19.3	6.3	37	0.5

value of soil and the rate of water extraction from the soil once the air entry has been exceeded, respectively; k is the hydraulic conductivity at any soil degree of saturation; and k_{sat} is the saturated hydraulic conductivity; the rest of the parameters have been defined earlier.

Table 3 lists the hydraulic characteristic parameters for all backfills determined using the van Genuchten–Mualem model in Equation (4). Figure 7 shows the

Table 3. Hydraulic characteristic parameters for studied backfills

Backfill	θ_s	θ_r	α (kPa ⁻¹)	n	k_{sat} (m/s)	ψ (kPa)
FC-0	0.38	0.02	0.382	4.30	1.00×10^{-4}	3.0
FC-6	0.44	0.02	0.603	4.02	7.80×10^{-5}	2.7
FC-19	0.51	0.06	0.169	3.74	1.10×10^{-6}	6.5
FC-30	0.40	0.04	0.623	1.25	5.00×10^{-7}	50
FC-60	0.33	0.10	0.024	2.19	1.85×10^{-7}	60

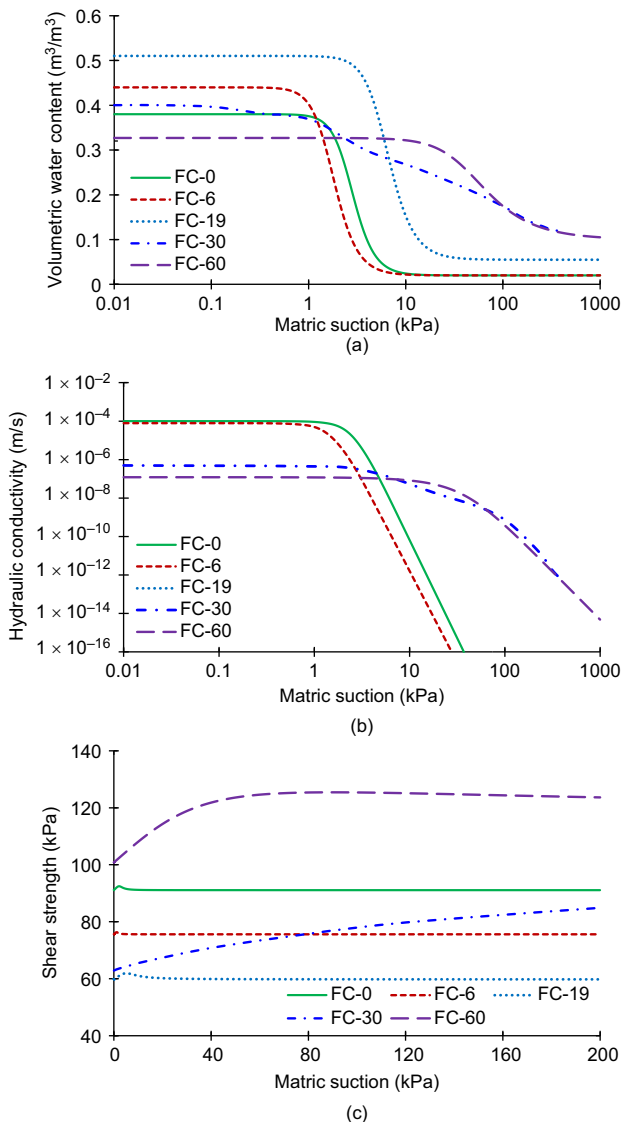


Figure 7. Hydraulic characteristics and shear strength of various backfills: (a) soil-water characteristic curves; (b) hydraulic conductivity functions; (c) shear strength at the base of the slope ($\sigma_n = 110$ kPa)

hydraulic characteristics and shear strength of backfills under unsaturated conditions. The unsaturated soil shear strength of the backfills in Figure 7c was predicted using Vanapalli’s function (Equation (1)) under normal pressure $\sigma_n = 110$ kPa, corresponding to the overburden pressure at the base of the slope. It can be observed that matric suction clearly had a significant influence on the shear strength of backfills with high fines content (FC > 19%). Using FC-60 as an example, when the matric suction varied from 0 to 50 kPa, the shear strength increased from 100 to 130 kPa. It should be noticed that the soil properties of the selected backfills in this study represent soils in general cases. Soils with the same amount of fines content could have different hydraulic and mechanical properties; hence, the numerical results based on the soil properties of the selected backfills presented in this study should be viewed in a comparative manner (i.e. comparing the results relatively among different backfills).

3.3. Reinforcement properties

The reinforcement tensile loads were incorporated into the equilibrium equation (balance of forces or moments) as the stabilizing forces in the slope stability analysis. The reinforcement tensile loads were assumed to be uniformly distributed with depth and to act horizontally on the failure surface. These assumptions are commonly employed in stability analyses of GRS structures (Duncan *et al.* 2014). Figure 8 illustrates the input tensile force distribution along the reinforcement length. The bilinear tensile force distribution along the reinforcement length was input based on its ability to provide rupture and pullout resistance. The rupture resistance was determined by the input reinforcement tensile strength, and the pullout resistance was calculated using the pullout equation.

$$P_r = R_c L_e (c'_a + \sigma'_v \tan \delta') \tag{6}$$

where P_r is the pullout resistance; $R_c (= 2)$ is the coverage ratio (or surface area factor), considering both the top and bottom surfaces of reinforcement; L_e is the horizontal distance to the free end of reinforcement; c'_a and δ' are the interface cohesion and friction angle, respectively, σ'_v is the effective overburden pressure on the reinforcement layer. As shown in Figure 8, the pullout resistance of the reinforcement increased linearly from zero at the free end of the reinforcement to a value equal to the input reinforcement tensile strength.

Table 4 lists the input values of reinforcement tensile strength T that were determined from the conventional

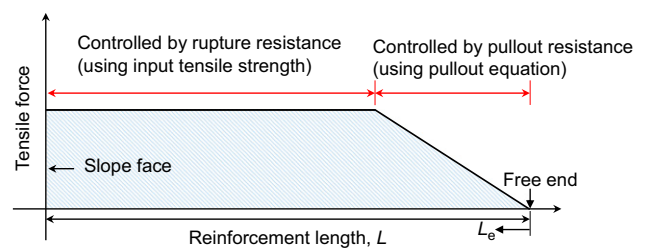


Figure 8. Schematic of input tensile force distribution along reinforcement length

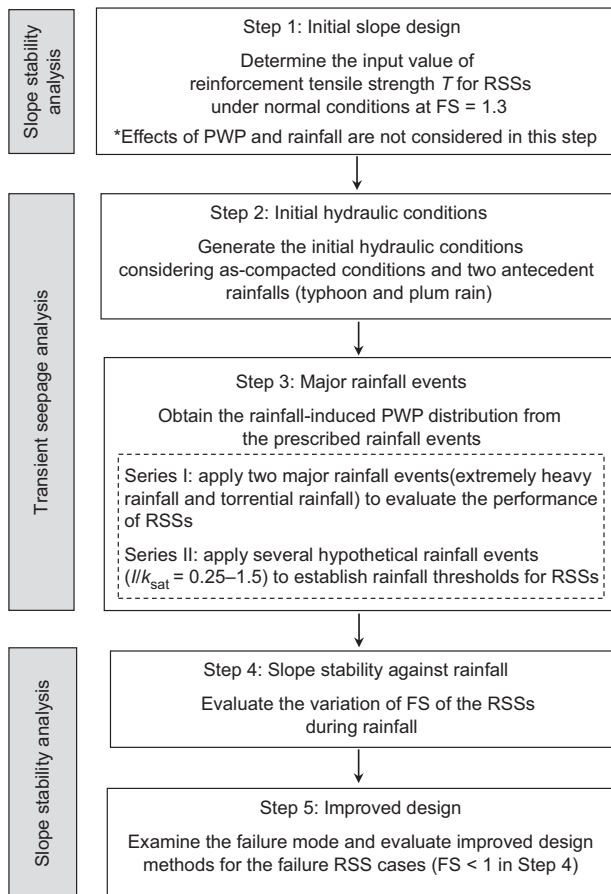


Figure 9. Flowchart of the analyses in this study

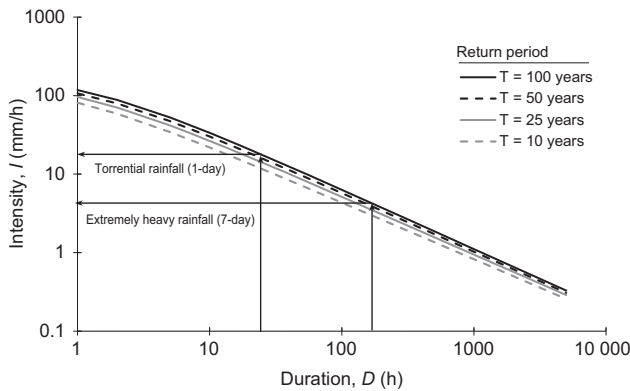


Figure 10. Intensity–duration–frequency curves for Taipei, Taiwan (redrawn from Cheng *et al.* 2001)

Horner’s, expressed as; formula

$$I = \frac{a_1}{(D + a_2)^{a_3}} \quad (7)$$

where I is extreme rainfall intensity; D is rainfall duration; a_1, a_2, a_3 are constants dependent on the return period and location. The values of constants in Horner’s formula for the Taipei area were adopted from the Taiwan handbook for hydrological design (Cheng *et al.* 2001). The rainfall intensities of two major rainfall events were determined from the I–D–F curve with a return period of 100 years because this duration covers the design lifetime of permanent GRS structures, 75–100 years, as recommended in design guidelines (Elias *et al.* 2001; Berg

et al. 2009). The determined rainfall intensities were $I = 4.3$ and 18.1 mm/h for the 7 and 1 day major rainfall events, respectively, which represent extremely heavy rainfall and torrential rainfall conditions as defined by the Taiwan Weather Bureau.

Figure 11 displays six rainfall scenarios considered in Series I, consisting of various combinations of initial conditions and major rainfall events. The rainfall scenarios in which as-compacted conditions were considered, along with typhoon and plum rain followed by 7 days of extremely heavy rainfall, are denoted as R1, R3, and R5, respectively; scenarios followed by 1 day of torrential rainfall are designated as R2, R4, and R6, respectively. The six rainfall scenarios were selected based on the likelihood of occurrence in chronological order and knowledge of local weather patterns. As Taiwan is situated in the Western Pacific typhoon region in which seasonal winds intersect, Taipei is exposed to a relatively high risk of natural disasters caused by heavy rainfall (annual average precipitation in Taipei City is 2663 mm/year in the plains and 4474 mm/year in the mountains). The selected rainfall scenarios involve multiple hazards including consecutive severe rainfall events, which often bring large volumes of precipitation and may cause disasters such as floods, landslides, and debris flows. For example, rainfall scenarios R3 and R4 represent the combined events of the typhoon and the moist south-westerly winds dragged by the passing of the typhoon. Rainfall scenarios R5 and R6 simulate the combined events of the plum rain followed by the summer seasonal winds or rainstorms. The purpose of the numerical analyses in Series I was to evaluate the hydraulic response and stability of the RSSs subjected to realistic rainfall scenarios. The variations of PWP and FS with time for each simulation case were compared and discussed. The failure cases from the numerical analyses in Series I were highlighted, and the improved design for these failure cases was assessed.

In Series II, several hypothetical rainfall events with a ratio of rainfall intensity to saturated soil hydraulic conductivity ranging from $I/k_{sat} = 0.25–1.5$ were applied to the RSSs. The simulations continued until slope failure occurred ($FS = 1$). The purpose of the numerical analyses in Series II was to evaluate the capacity of RSSs to endure the demands of continued rainfall. The rainfall threshold curves for the RSSs were established, and were determined based on the applied rainfall intensity and duration at $FS = 1$. The established rainfall thresholds (as the system resistance against rainfall) were further compared with the regional I–D–F curves (as the system potential driving forces), which could provide a simplified and robust method to assess the failure risk of RSSs and to facilitate backfill selection in accordance with regional hydrological conditions.

The numerical analyses were performed in five main steps (Figure 9). First, conventional slope stability analyses (without considering the effect of PWP and rainfall) were performed to determine the input value of reinforcement tensile strength at $FS = 1.3$. Second, transient seepage analysis was performed to generate the initial hydraulic conditions (i.e. initial PWP distribution). Third, subsequent transient seepage analysis was conducted to obtain the rainfall-induced PWP distribution from major

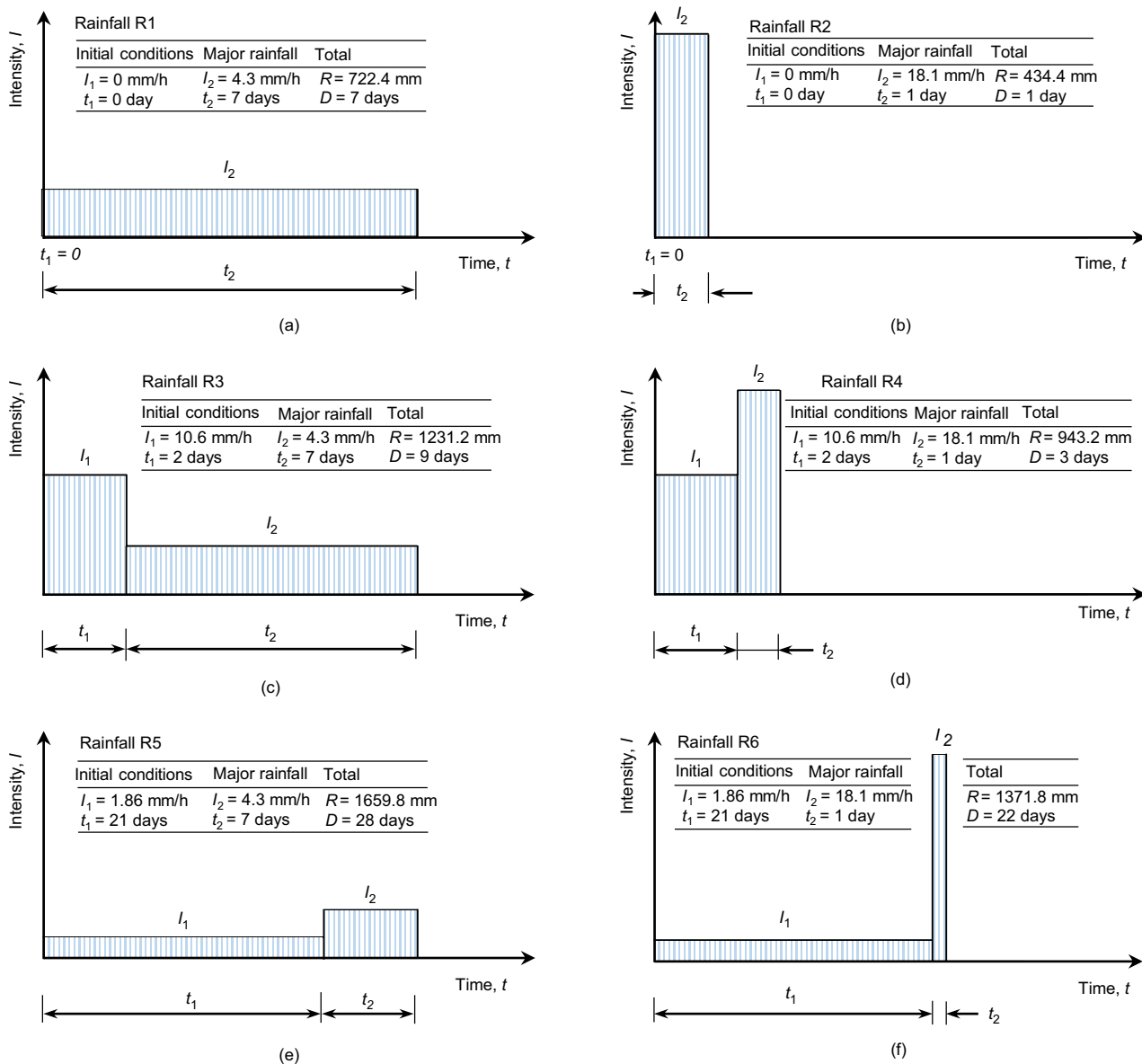


Figure 11. Applied rainfall scenarios consisting of initial conditions and major rainfall: (a), (c), and (e) as-compacted conditions, typhoon, and plum rain, respectively, followed by 7-day extremely heavy rainfall; (b), (d), and (f) as-compacted conditions, typhoon, and plum rain, respectively, followed by 1-day torrential rainfall

rainfall events. Fourth, the predicted PWP during rainfall was incorporated into the slope stability analysis to calculate the corresponding FS at various rainfall stages. Fifth, the failure mode of the failure RSS cases under prescribed rainfall scenarios was examined and the improved design methods were evaluated. As the same as the limit equilibrium calculation performed in model validation, Spencer’s method, which rigorously satisfies all three equilibrium conditions (i.e., vertical force, horizontal force, and moment equilibrium), was selected to calculate the FS of RSSs. A circular failure surface was specified to search for the critical failure surface based on the observations from several failure case studies that found the failure surface of GRS structures in the field was close to a circular shape. (Yoo and Jung 2006; Liu *et al.* 2012; Miyata and Shinoda 2016; Yang *et al.* 2019). Further, the optimization function, as coded in SLOPE/W, was also adapted to produce a more

realistic failure surface shape and to obtain the most critical FS value.

3.5. Influence of rainfall patterns

Many studies have shown that rainfall patterns can affect the mechanism and occurrence (or failure timing) of shallow landslides on natural slopes (Rahimi *et al.* 2011; Tsai and Wang 2011; Muntohar *et al.* 2013; Suradi and Fourie 2014; Ran *et al.* 2018). A preliminary parametric study was conducted to examine the influence of the rainfall patterns of the major rainfall events on the PWP distribution and slope stability of the RSSs. Using the slope model with FC-30 subjected to rainfall scenario R3 as an example (Figure 12), four representative rainfall patterns were considered: delayed, advanced, normal (centralized), and uniform. In these rainfall patterns, the total accumulated rainfall of $R = 722.4$ mm corresponded to an intensity of 4.3 mm/h over the 7 days of the

extremely heavy rainfall event, and it was distributed according to the shape of the rainfall pattern.

Figure 13a shows the variation of PWP with time for various applied rainfall patterns. The PWP value was monitored at the slope base located below the crest of the slope, as indicated in Figure 5. The results revealed that PWP remained largely the same for all the rainfall patterns before $t = 144$ h. After this time, PWP began to deviate as it rapidly increased. At the end of major rainfall ($t = 216$ h), the RSSs subjected to the uniform and advanced rainfall patterns experienced the largest increase in PWP (i.e. loss of

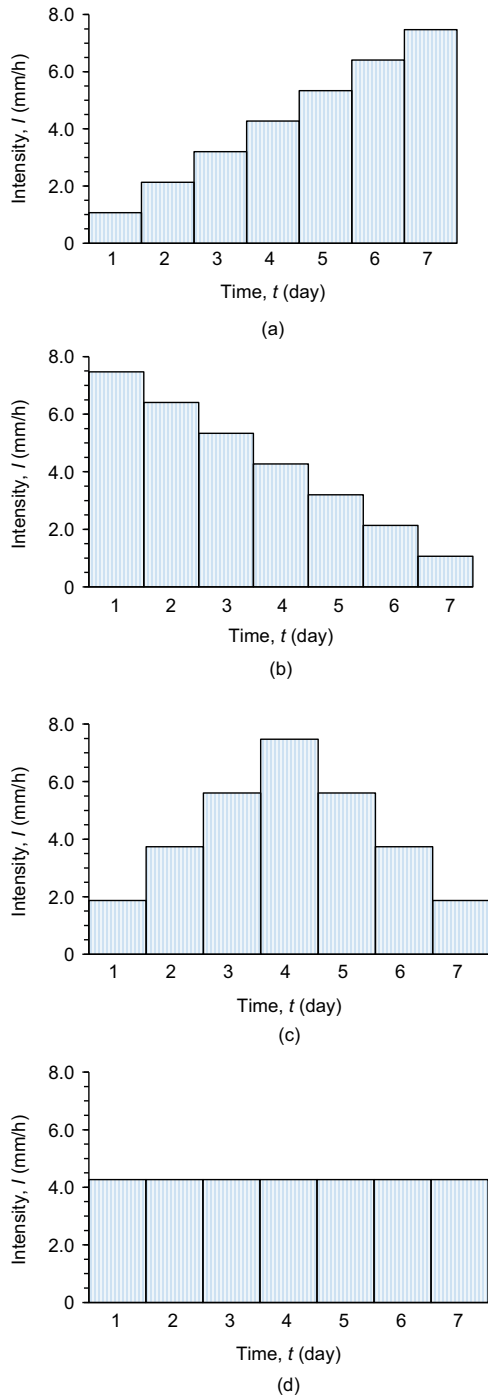


Figure 12. Rainfall patterns using extremely heavy rainfall as an example: (a) delayed pattern; (b) advanced pattern; (c) normal pattern; (d) uniform pattern

matric suction), whereas the RSS subjected to the delayed rainfall patterns had the least increase in PWP.

Figure 13b shows the variation of FS with time for various applied rainfall patterns. The FS values for all the applied rainfall patterns gradually decreased as rainfall infiltration proceeded. After major rainfall, the RSSs subjected to the uniform and advanced rainfall patterns had the lowest FS value as they developed the correspondingly largest PWP. Tsai and Wang (2011) investigated the influence of rainfall patterns on the occurrence of shallow landslides and reached the same conclusion. They found that the landslides occurred earliest under the uniform rainfall pattern, followed by advanced rainfall pattern, and then centralized rainfall pattern. Rahimi *et al.* (2011) reported similar findings that among three evaluated rainfall patterns (delayed, normal, and advanced), the advanced rainfall pattern resulting in the lowest minimum FS for the slope with low soil permeability.

The influence of rainfall patterns on the PWP development and slope stability of RSSs is a complex rainfall-soil interaction problem because both the rainfall intensity and unsaturated soil permeability could vary with time. This mutually variable relationship between the rainfall intensity and soil permeability determines not only the amount but also the rate of rainfall infiltration at each time step of rainfall, which could further affect the accumulation of PWP within a slope. At a certain time step of rainfall, if the rainfall intensity is less than the soil permeability, the rainfall infiltration rate is low (because of small inflow flux from rainfall) but the entire amount of rainfall can infiltrate into the soil. Conversely, if the rainfall intensity is greater than the soil permeability, the rainfall infiltration rate is high but the excessive rainwater turns into runoff and does not enter the slope. As rainfall proceeds, the cumulative difference due to the contrasting effect of the amount and the rate of rainfall infiltration at each time increment causes different PWP and FS values for the slopes under different rainfall patterns. Based on the numerical results in the preliminary parametric study, among all the applied rainfall patterns, the uniform and advanced rainfall patterns have the greatest influence on PWP development and slope stability. Accordingly, this study chose the uniform rainfall pattern with constant rainfall intensity for the numerical analyses to obtain the most critical results.

4. RESULTS AND DISCUSSION

4.1. Variation of porewater pressure

The numerical results of Series I, the hydraulic response and stability of the RSSs subjected to the six applied rainfall scenarios, were evaluated and discussed. The development of PWP within the RSSs is presented in terms of the porewater pressure coefficient (r_u), defined as

$$r_u = \frac{u}{\gamma H} \tag{8}$$

where u is the PWP at the slope base located vertically below the crest of slope (as indicated in Figure 5); γ is the soil unit weight, and H is the height of the slope. As expressed in Equation 8, the r_u parameter is defined as the

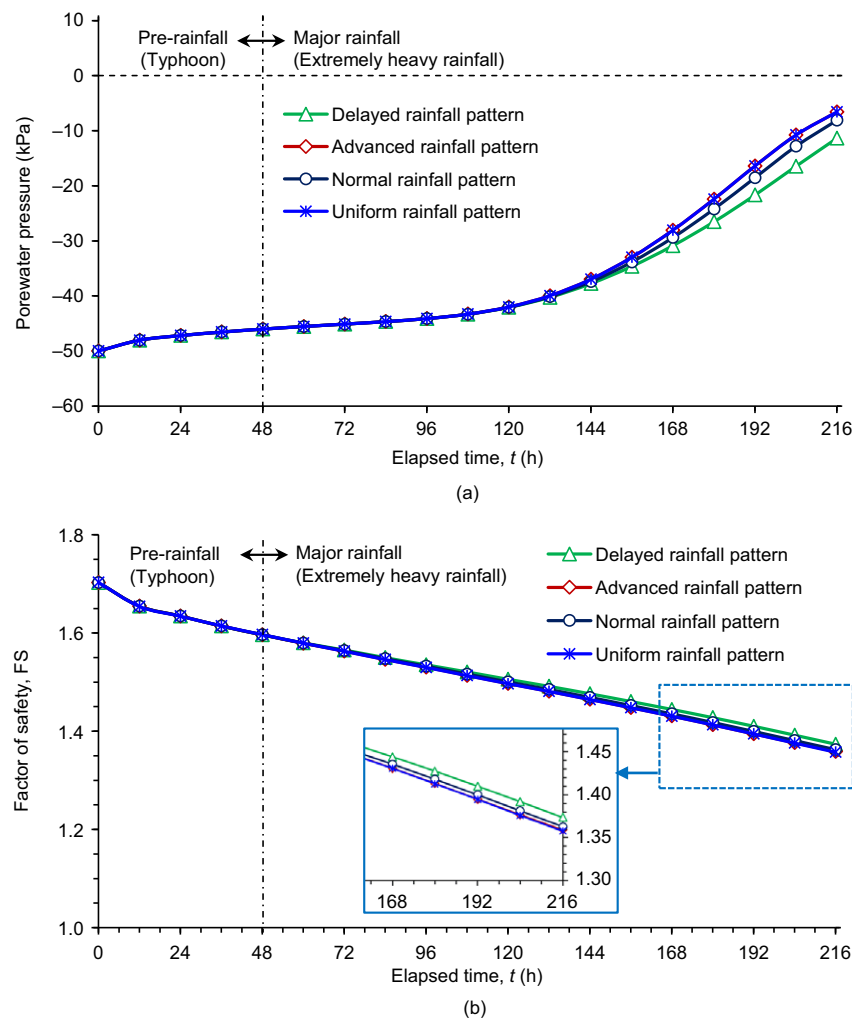


Figure 13. Effect of rainfall pattern on porewater pressure and factor of safety of RSS with FC-30

ratio of the porewater pressure to the overburden stress at a certain depth of interest in a slope. It is a well-known dimensionless parameter for a slope stability analysis used to represent the normalized porewater pressure condition within a slope (Duncan *et al.* 2014). The main reason for using the r_u parameter in this study is to present normalized porewater pressure values that are independent of the height of the slope. In this study, the r_u value at the base under the crest was selected to examine the influence of the build-up of positive PWP from the bottom of the slope under rainfall infiltration. The calculated r_u value at this location represents approximately the average porewater value along the base of the slope.

Figures 14 and 15 present the variation of r_u with time under different initial conditions followed by 7 days of extremely heavy rainfall and 1 day of torrential rainfall, respectively. Table 5 summarizes the maximum r_u values obtained at the base under the crest for each rainfall scenario. As shown in Figures 14 and 15, at the beginning of the simulation ($t = 0$ h), all of the RSSs were under partially-saturated conditions with negative r_u values corresponding to the as-compacted matric suctions of the backfills. The r_u values of RSSs with FC-0 and FC-6 (i.e. low fines content) increased rapidly in response to the applied rainfall, indicating that rainfall infiltration quickly reached the

base of the slope. As rainfall progressed, the r_u values increased and became slightly larger than zero, indicative of the development of small positive PWPs. Because of the high permeability of these two backfills ($I/k_{sat} \ll 1$ as indicated in Table 5), after the maximum r_u value was reached, the r_u values started to decrease (i.e. dissipation of PWP out of the backfills) or remained constant (i.e. equilibrium between inflow and outflow at steady state). Figures 14 and 15 clearly show that the applied rainfall scenarios had little influence on the development of the PWP within RSSs with these two backfills. As listed in Table 5, for the six applied rainfall scenarios, the maximum r_u values fell within a small range: $r_u = 0.08$ – 0.13 and 0.0 – 0.08 for the RSSs with FC-0 and FC-6, respectively.

Compared with the RSSs with low fines content backfills, the PWP within RSSs with FC-19, FC-30, and FC-60 (i.e. high fines content) had a delayed response to the applied rainfall because these three backfills had relatively low permeability ($I/k_{sat} > 1$ as indicated in Table 5). The PWP within RSSs with FC-19, FC-30, and FC-60 exhibited two contrasting responses, depending on the total duration of the applied rainfall scenarios:

- For rainfall scenarios R1, R2, and R4, which had short rainfall durations ($D = 168, 24,$ and 72 h, respectively),

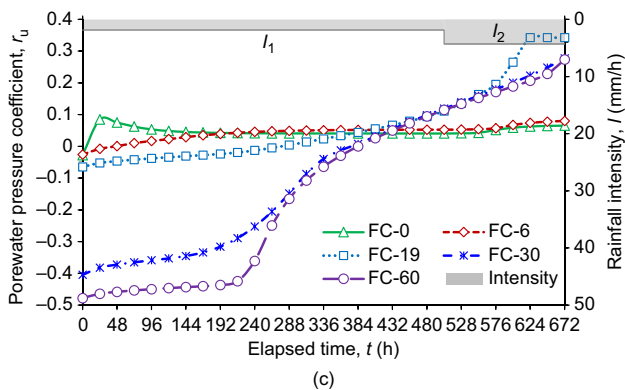
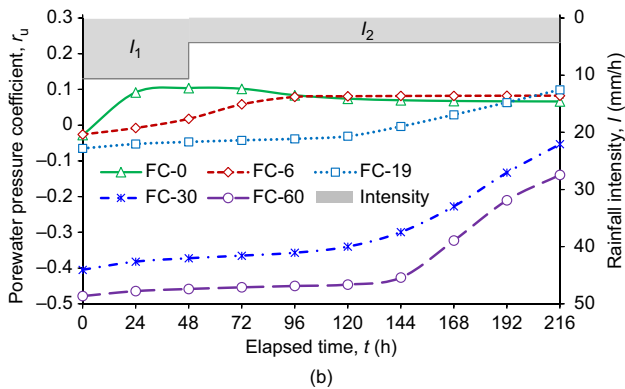
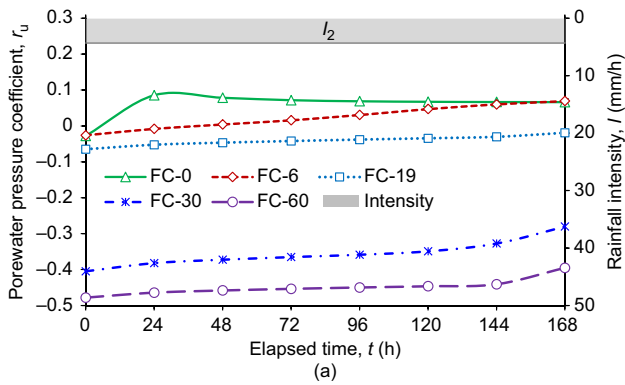


Figure 14. Variation of porewater pressure coefficient with time under different initial conditions followed by extremely heavy rainfall for scenarios of (a) R1; (b) R3; and (c) R5

the r_u values showed no change or a slight increase (Figures 14a, 15a and 15b). This is because the wetting front had yet to or had just reached the base of the slope, thus causing insignificant PWP variation before the end of the rainfall event. Negative PWP remained in the RSS during the entire rainfall event.

- For rainfall scenarios R3, R5, and R6, which had long rainfall durations ($D = 216, 672,$ and 528 h, respectively), the r_u values showed a substantial increase during rainfall (Figures 14b, 14c and 15c). The rapid increase in the r_u values occurred during the antecedent rainfall in R5 and R6 and during the major rainfall event in R3. Because the inflow flux (i.e. I) was higher than the outflow flux (limited by the k_s of the backfill), continued rainfall resulted in the initial negative PWP (or matric suction) gradually disappearing with the passage of the wetting front,

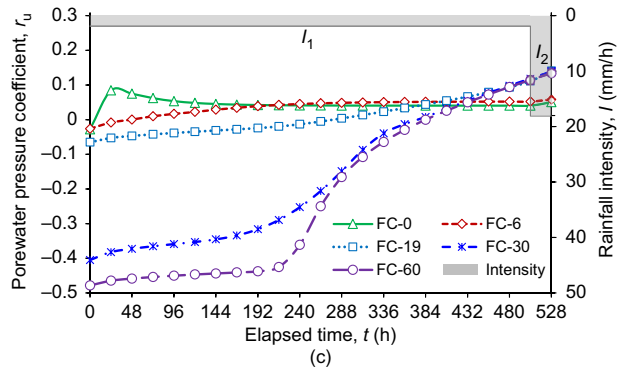
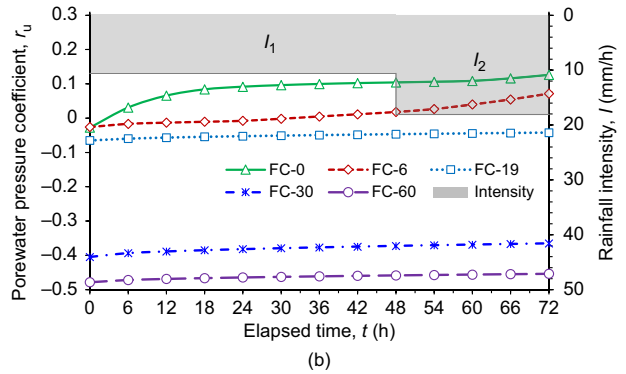
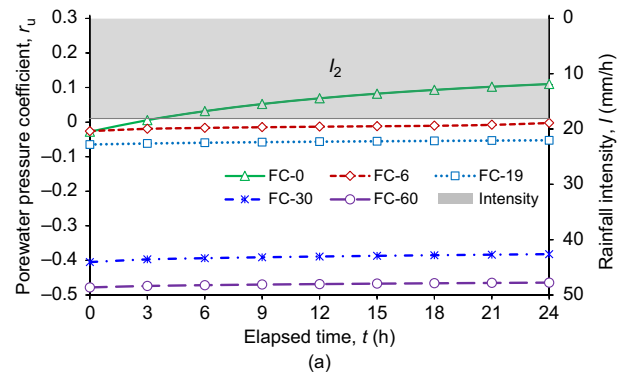


Figure 15. Variation of porewater pressure coefficient with time under different initial conditions followed by torrential rainfall for scenarios of (a) R2; (b) R4; and (c) R6

where eventually the backfill became completely saturated and positive PWP developed.

Figure 16 shows the relationship between the developed maximum PWP and the total rainfall duration of the rainfall scenario for RSSs with backfills containing high fines content ($FC \geq 19\%$). A clear increase in PWP was observed at the total rainfall duration $D = 216$ h, and the development of PWP became highly correlated to the total rainfall duration when $D > 216$ h. Figure 17 presents an overall comparison of the maximum r_u values for various backfills and rainfall scenarios. The critical r_u values responsible for slope failure ($FS = 1$) are also labeled for reference. Notably, the maximum r_u values vary significantly with the applied rainfall scenarios for the RSSs with FC-19, FC-30, and FC-60. Not all the rainfall conditions had an adverse impact on the RSSs with backfills containing high fines content. As discussed previously, negative r_u values remained when considering

Table 5. Summary of numerical results from Series I

Backfill	Initial conditions	Extremely heavy rainfall, $I = 4.3$ (mm/h)			Torrential rainfall, $I = 18.1$ (mm/h)		
		Ilk_{sat}	r_u	FS	Ilk_{sat}	r_u	FS
FC-0	As compacted	0.01	0.09	1.34	0.05	0.11	1.32
	Typhoon		0.11	1.33		0.13	1.31
	Plum rain		0.09	1.34		0.09	1.34
FC-6	As compacted	0.02	0.07	1.31	0.06	0.00	1.32
	Typhoon		0.08	1.30		0.07	1.31
	Plum rain		0.08	1.30		0.06	1.31
FC-19	As compacted	1.08	-0.02	1.34	4.58	-0.05	1.40
	Typhoon		0.10	1.25		-0.04	1.37
	Plum rain		0.34	0.73 (CF ^a)		0.14	1.26
FC-30	As compacted	2.37	-0.28	1.45	10.07	-0.38	1.63
	Typhoon		-0.05	1.36		-0.37	1.56
	Plum rain		0.28	0.99 (CF ^a)		0.140	1.24
FC-60	As compacted	6.41	-0.40	1.74	27.21	-0.46	2.43
	Typhoon		-0.14	1.60		-0.45	2.29
	Plum rain		0.27	0.87 (IF ^b)		0.13	1.23

^aCompound failure.

^bInternal failure.

Bold values aim to emphasize FS value less than 1 as slope failure. Other values are acceptable.

some simulated rainfall conditions with short durations, whereas positive r_u values developed under the rainfall conditions with long durations. The RSSs with high fines content backfills developed high positive PWP under the combined effects of plum rain and 7 days of extremely heavy rainfall (i.e. rainfall scenario R5), which had the longest duration ($D = 672$ h). Under rainfall scenario R5, the maximum r_u values were 0.34, 0.28, and 0.27 for the RSSs with FC-19, FC-30, and FC-60, respectively (Table 5). The developed maximum r_u values exceeded the critical value, indicating that the slope was unstable. This finding confirms that GRS structures with high fines content backfills should be designed with special caution to prevent the accumulation of high PWP within such backfills when subjected to rainfall.

4.2. Slope stability and variation of factor of safety

Figures 18 and 19 present the variation of FS with time under different initial conditions followed by 7 days of extremely heavy rainfall and 1 day of torrential rainfall, respectively. Table 5 summarizes the calculated minimum FS values for each rainfall scenario. Initially ($t = 0$ h), the FS increased as the fines content of the backfill increased. This is because high initial as-compacted matric suction in the marginal backfill (Table 3) contributed to an increase in soil shear strength, leading to an increase in slope stability. Although the FSs of RSSs with FC-0 and FC-6 were initially low, the FS values were almost constant during rainfall. This is because the shear strength of these two backfills exhibited a negligible change with matric suction (Figure 7c), and the high permeability of the backfills prevented the RSSs from becoming completely saturated; thus, the RSSs with these two backfills maintained stability under the prescribed rainfall conditions. In addition, the influence of the applied rainfall scenarios on the FS values of RSSs with these two backfills

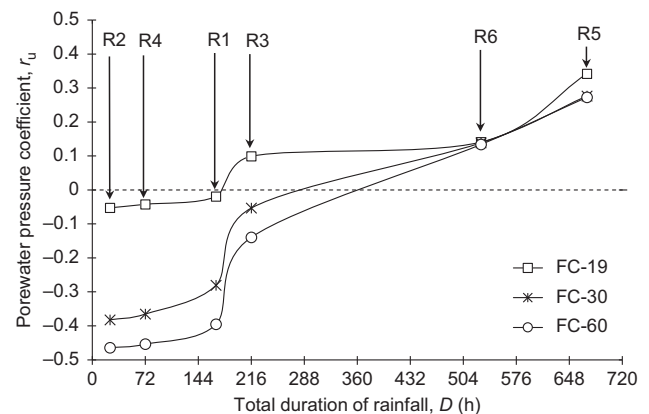


Figure 16. Relationship between developed maximum PWP and the total duration of the rainfall scenario for RSSs with high fines content backfills

was generally negligible. As listed in Table 5, for the six applied rainfall scenarios, the minimum FS values fell in a small range: FS = 1.31–1.34 and 1.30–1.32 for the RSSs with FC-0 and FC-6, respectively. In summary, the initial soil saturation conditions and rainfall infiltration considered in the simulation had a negligible influence on the stability of the RSSs with high-quality backfills, which have low fines content. This finding supports the free-draining conditions assumed in conventional design methods for GRS structures with high-quality backfills, in which the effect of PWP is not considered in the design.

For the RSSs with FC-19, FC-30, and FC-60, the FS values were initially high because of high initial matric suction and decreased with time as rainfall progressed. The applied rainfall scenarios considerably affected the calculated FS values. For example, the decrease in FS was negligible for rainfall scenario R2, which had the shortest

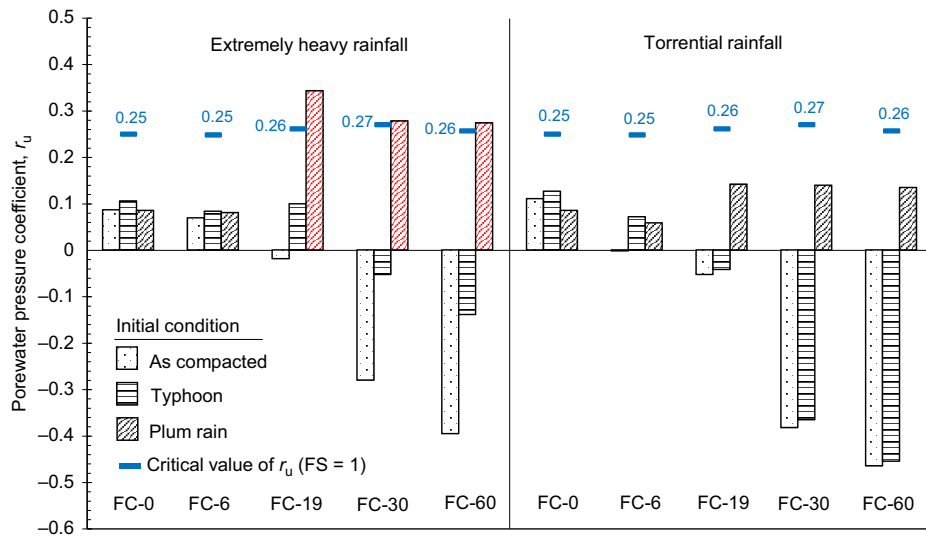


Figure 17. Summary of maximum and critical porewater pressure coefficients for each scenario

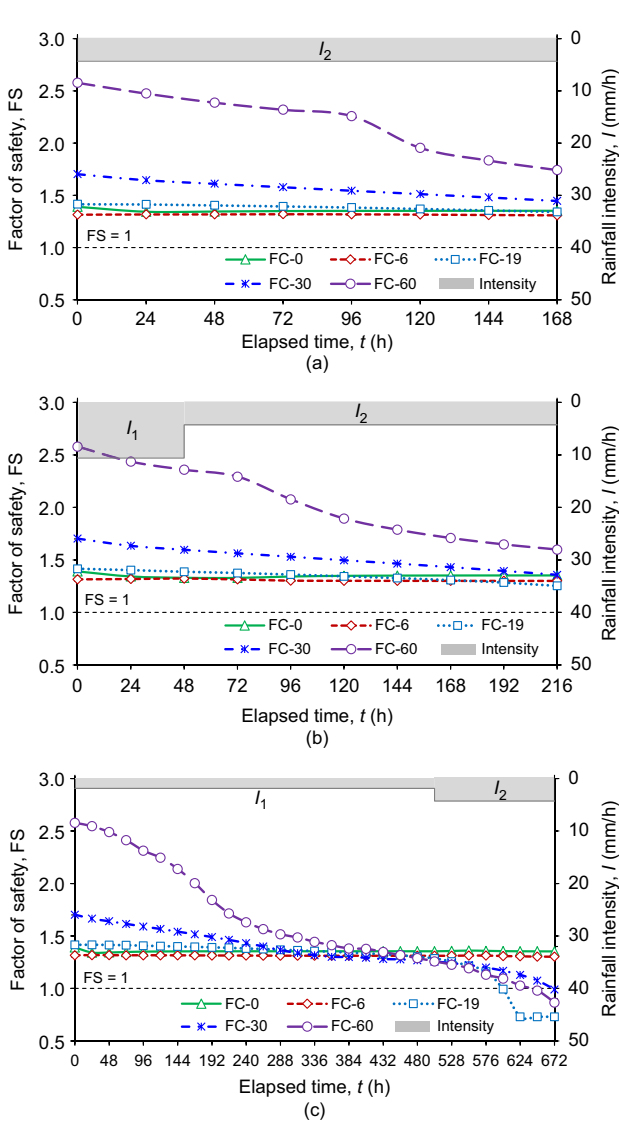


Figure 18. Variation of FS with time under different initial conditions followed by extremely heavy rainfall for scenarios of (a) R1; (b) R3; and (c) R5

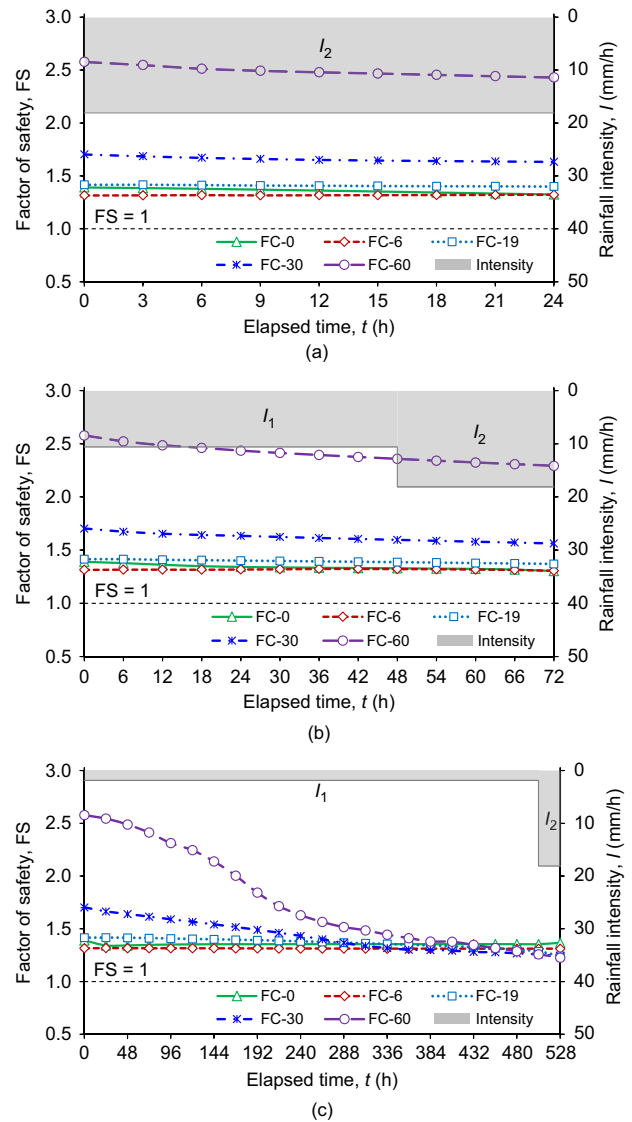


Figure 19. Variation of FS with time under different initial conditions followed by torrential rainfall for scenarios of (a) R2; (b) R4; and (c) R6

duration $D=24$ h (Figure 19a), whereas the decrease in FS was pronounced for rainfall scenario R5, which had the longest duration $D=672$ h (Figure 18c). This difference was attributed to the development of PWP associated with the total duration of the applied rainfall scenario, as discussed previously.

Among all the applied rainfall scenarios, slope failure ($FS < 1$) of the RSSs with high fines content backfills ($FC \geq 19\%$) occurred only under rainfall scenario R5 (Figure 18c). The RSSs with FC-19, FC-30, and FC-60 failed (FS reached 1) at 600, 670, and 640 h after the rainfall started, respectively, resulting from the build-up of high positive PWP at the base of the slope exceeding the critical r_u value (Figure 17). The numerical results suggest that the PWP development and stability of RSSs using high fines content soil as backfill are sensitive to different rainfall conditions. The regional hydrological conditions, especially for rainfall events with prolonged duration, should be considered in the design of GRS structures when marginal soil is used as backfill.

4.3. Failure mode and improved design

The failure modes of the failure cases (RSSs with FC-19, FC-30, and FC-60 under rainfall scenario R5) were examined. As shown in Figure 20, the three failed RSSs were fully saturated and high positive PWP developed within their backfills. At the moment of failure, the phreatic level had risen to the top of the slope. Compound failure modes were found in the RSSs with FC-19 and FC-30, in which the failure surface passed beyond the reinforced zone and into the retained soil. An internal failure mode caused by reinforcement rupture occurred in the RSS with FC-60 because the relatively low input reinforcement tensile strength ($T=3.2$ kN/m) for this case allowed the failure surface to cut through all of the reinforcement layers.

The improved design methods for the RSSs against rainfall were further assessed. These failed slopes were redesigned by either increasing the reinforcement tensile strength or reinforcement length, depending on the failure mode, to achieve $FS = 1.1$ under the prescribed rainfall

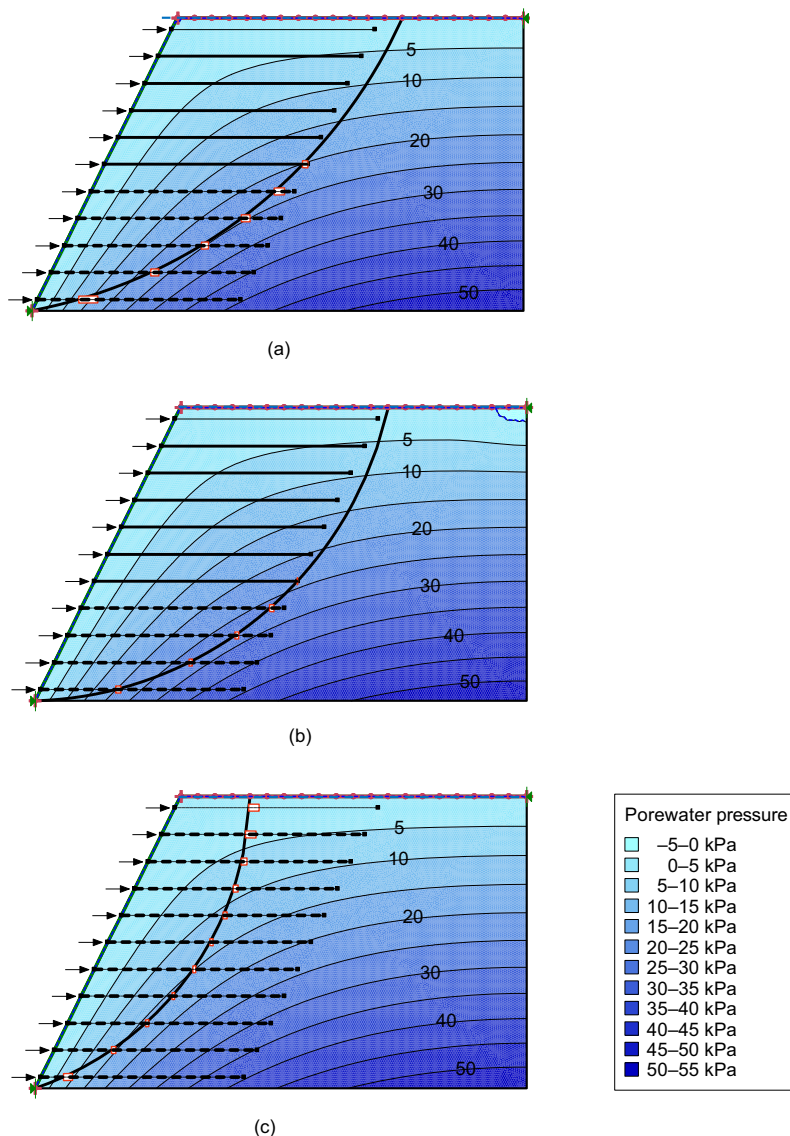


Figure 20. Failure modes and porewater pressure contours for RSSs with (a) FC-19; (b) FC-30; and (c) FC-60

conditions. Table 6 lists the results of the improved design against rainfall. For the RSSs with FC-30 and FC-60, the reinforcement tensile strength had to be increased by 2.75 and 2.06 times to $T = 12.1$ and 6.58 kN/m, respectively, to satisfy $FS = 1.1$ under the prescribed rainfall conditions. The improved designs for the RSSs with FC-30 and FC-60 resulted in corresponding $FS = 1.48$ and 1.64 , respectively, under normal conditions (without considering the effects of soil matric suction and rainfall).

For the RSS with FC-19, increasing only the T value, in this case, seemed to be ineffective in increasing the FS to the designated value. As the T value increased, the potential failure surface extended deep into the retained zone, resulting in little mobilized tensile resistance of reinforcement layers within the critical failure surface, limiting the contribution of reinforcements towards system stability. The effect of decreasing reinforcement spacing S_v on improving FS was further evaluated. The numerical results indicate that the FS value slightly increases from 0.73 to 0.92 when the S_v decreases from 0.6 to 0.2 m. The target slope stability ($FS = 1.1$) under the prescribed rainfall condition still cannot be achieved even at $S_v = 0.2$ m, the minimum reinforcement spacing that could be constructed practically (Wu 2019). Similar to the findings from the method of increasing T , the decreasing S_v seemed also to be an ineffectual improvement method for the slope in this case, where the dominant failure mode was a compound failure. To rectify this problem, in addition to increasing the reinforcement tensile strength, the reinforcement length may be increased. As shown in Table 6, to satisfy $FS = 1.1$ under the prescribed rainfall conditions, the reinforcement tensile strength was increased 2.98 times to $T = 22.5$ kN/m, and the reinforcement length was increased 1.42 times to $L = 6.5$ m ($L/H = 1.0$). The corresponding FS of this improved design was 2.10 under normal conditions.

Evaluation of the criteria that may be used to improve the design of RSS under rainfall conditions highlights why many GRS structures fail under compound or deep-seated failure modes instead of internal failure modes when subjected to rainfall, as reported in the literature (Table 1). Such failures occur because the reinforcement tensile strength is often conservatively designed considering the reduction factors for creep, durability, and installation damage and FS against internal breakage. By contrast, the shear strength of both reinforced backfill and retained

soil can substantially decrease when subjected to rainfall infiltration. Consequently, the critical failure surface avoids intersecting with as many reinforcement layers as possible to minimize the FS , which therefore prevents the occurrence of internal failure. Depending on the relative magnitude of the reinforcement tensile strength and soil shear strength, the failure surface may only cut through part of the reinforcement layers (i.e. a compound failure mode) or even completely avoid intersecting with any reinforcement layers (i.e. a deep-seated failure mode). The results of this design exercise also highlight that the reinforcement length is an important variable for the design of RSSs against rainfall. Increasing the reinforcement length can prevent the extension of potential failure surfaces backward into the retained zone, and thus more reinforcement layers can effectively contribute to increasing system stability.

4.4. Rainfall threshold for RSS

The numerical results of Series II are discussed herein. The capacity of the RSSs to endure rainfall was evaluated to establish the rainfall threshold (i.e. the critical rainfall intensity and duration required to cause slope failure) for the RSSs with various backfills and initial conditions. The established rainfall thresholds as the system resistance against rainfall were further compared with the regional I–D–F curves as the system potential driving forces. As shown in Figure 21, if the calculated rainfall threshold lies above the I–D–F curve (i.e. the resistance is larger than the driving force), RSSs can maintain their stability under the regional potential rainfall. Conversely, if the calculated rainfall threshold falls below the I–D–F curve (i.e. the driving force is larger than the resistance), RSSs can potentially fail during rainfall in a specific region.

As shown in Figure 21, the rainfall thresholds for the RSSs with high-quality backfills (i.e. FC-0 and FC-6) exhibited a high intensity–short duration characteristic for failure, whereas those for the RSSs with high fines content backfills (i.e. FC-19, FC-30, and FC-60) exhibited a low intensity–long duration signature. When the rainfall intensity increased beyond the infiltration capacity of the soil (i.e. $I \geq k_s$), the rainfall threshold curve exhibits a concave-up shape, as shown in Figure 21. This is because when $I \geq k_s$, the excessive rainwater became runoff and did not enter the slope to increase the PWP. Consequently, the time taken for the RSS to fail did not change when $I \geq k_s$. In addition, the rainfall threshold had a lower limit of rainfall intensity ($I/k_s = 0.2–0.4$ for RSSs with high fines content backfills). When the applied rainfall intensity was less than this lower limit, RSS failure did not occur because the low-intensity rainfall was insufficient to saturate the backfill completely regardless of the duration of the rainfall applied.

As shown in Figure 21, the rainfall thresholds of the RSSs with high-quality backfills were marginally influenced by the initial conditions. All rainfall thresholds for the RSSs with high-quality backfills were above the I–D–F curves, indicating that at a given rainfall duration, the rainfall intensity required to cause slope failure exceeded the rainfall intensity that could possibly occur in

Table 6. Improved design parameters accounting for rainfall conditions considered in this study

Backfill	Original design			Modified design ^a		
	T (kN/m)	L/H	FS	T (kN/m)	L/H	FS^b
FC-19	7.55	0.7	1.3	22.5	1.0	2.10
FC-30	4.4	0.7	1.3	12.1	0.7	1.48
FC-60	3.2	0.7	1.3	6.58	0.7	1.64

^aThe improved design is to achieve $FS = 1.1$ under the prescribed rainfall conditions.

^bThe corresponding FS value under normal conditions.

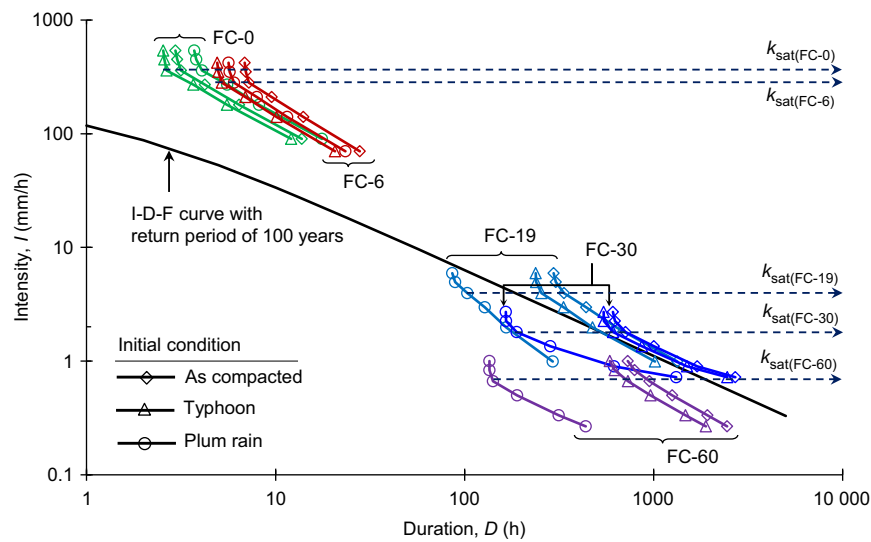


Figure 21. Rainfall thresholds of reinforced slopes with various backfills and different initial conditions

that region. Thus, the RSSs with high-quality backfills are expected to remain stable under the regional rainfall conditions over 100 years of recurrence. By contrast, the rainfall thresholds of the RSSs with high fines content backfills were significantly influenced by the initial conditions. The rainfall thresholds shifted parallel to the right as the duration of the antecedent rainfall in the initial conditions increased. When the prolonged initial conditions (i.e. plum rain) were considered, the rainfall thresholds of the RSSs with high fines content backfills fell below the I–D–F curves, suggesting that these RSSs could fail when subjected to the potential regional rainfall.

Comparison of established rainfall thresholds with regional I–D–F curves provides a simplified and robust method for assessing the failure risk of RSSs and facilitating backfill selection in accordance with regional hydrological conditions. For example, the information in Figure 21 reveals that soil with fines content $FC \geq 19\%$ was unsuitable for use as backfill for this RSS design because it would have a risk of failure when subjected to

the regional rainfall across its design lifespan. In this case, either the RSS should be redesigned or backfill with lower fines content should be adopted to improve the stability of the RSS against rainfall.

To verify the proposed concept, the rainfall thresholds of three failure cases with compound failure modes (Cases 3, 4, and 5 in Table 1) were analyzed on the basis of the reported rainfall data. The other failure cases in Table 1 were not included because Cases 1 and 2 have incomplete rainfall data reported in the literature and Cases 6 and 7 have deep-seated failure modes that are mainly controlled by the in situ geological conditions and are irrelevant to the backfill selection and reinforcement design of GRS structures. Figure 22 shows comparisons between the rainfall thresholds of the selected failure cases and the regional I–D–F curves in the locations where the GRS structures were built. All of the rainfall thresholds of the failure cases lay below the I–D–F curves for each region, indicating that the failure of these GRS structures may occur under regional hydrological conditions. This is

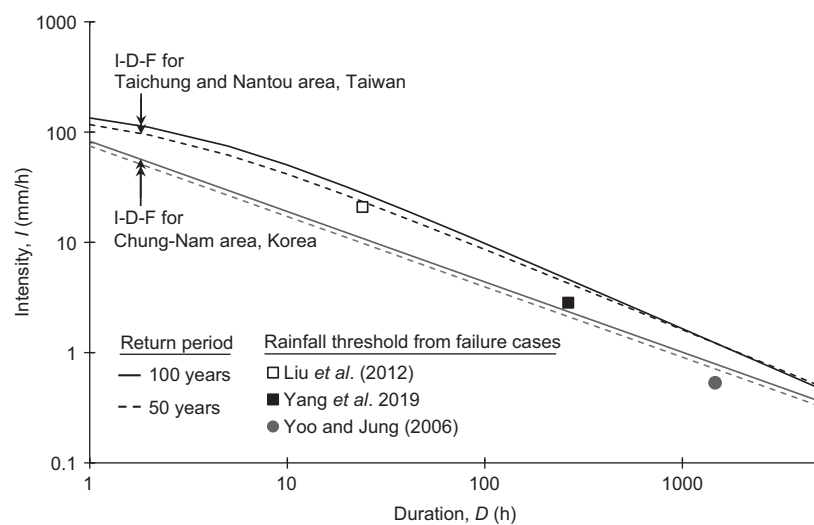


Figure 22. Comparison between the rainfall thresholds of failure cases and the regional I–D–F curves

reasonable, because these GRS structures actually failed due to rainfall in each region. The comparison presented in Figure 22 validates the proposed concept for the design of GRS structures against rainfall considering regional hydrological conditions.

5. CONCLUSION

This study presented a series of numerical analyses that coupled various geotechnical parameters with hydrological conditions to investigate the impact of rainfall on performance and design of RSSs. The effects of backfill fines content, soil initial matric suctions, and rainfall scenarios on the hydraulic response and stability of RSSs were evaluated. The rainfall threshold for RSSs was established to provide a simplified and robust method for designing RSSs against rainfall. This study highlights the importance and need for considering regional hydrological conditions for the design of GRS structures, especially when marginal soil is used as backfill. The following conclusions can be drawn from the results presented in this study.

- (1) The numerical model was validated using a well-documented failure case history of a GRS wall. The model validation demonstrated that numerical analysis based on a framework of unsaturated soil mechanics can accurately predict the failure timing and failure mechanism of GRS structures under rainfall infiltration.
- (2) Among all the rainfall patterns, the use of uniform and advanced rainfall patterns under a given total accumulated rainfall leads to the most critical results, the highest PWP and lowest of the RSSs.
- (3) The applied rainfall scenarios had little influence on the performance of RSSs with high-quality backfills (i.e. FC-0 and FC-6), whereas prolonged rainfall durations substantially compromised the performance of RSSs with high fines content backfills (i.e. FC-19, FC-30, and FC-60).
- (4) Depending on the total duration of the applied rainfall scenarios, the hydraulic response and stability of the RSSs with high fines content backfills exhibited two contrasting responses. The PWP and FS of the RSSs exhibited no variation or slight variation for rainfall scenarios with short rainfall durations (i.e. R1, R2, and R4), whereas the PWP and FS of the RSSs significantly changed for rainfall scenarios with long rainfall durations (i.e. R3, R5, and R6).
- (5) The RSSs with high fines content backfills (FC \geq 19%) developed high positive PWP under the combined effects of the plum rain and 7 days of extremely heavy rainfall (i.e. rainfall scenario R5), which had the longest duration ($D = 672$ h). The developed maximum r_u values exceeded the critical value, and thus RSS failure occurred under this specific rainfall scenario.
- (6) The results of the improved design analysis highlighted that reinforcement length is also an

important variable when designing RSSs against rainfall, especially when compound failure modes dominate RSS instability. Increasing the reinforcement length can prevent the extension of the potential failure surface backward into the retained zone, and thus more reinforcement layers can effectively contribute, thereby increasing system stability.

- (7) Rainfall thresholds with high intensity–short duration were determined for RSSs with high-quality backfills, whereas those with low intensity–long duration were found for RSSs with high fines content backfills. All rainfall thresholds for the RSSs with high-quality backfills lay above the I–D–F curves, indicating that the designed RSSs were expected to remain stable under the regional rainfall conditions. The initial conditions could significantly influence the rainfall thresholds of the RSSs with high fine content backfills. When the prolonged initial conditions (i.e. plum rain) were considered, the rainfall thresholds of the RSSs with high fines content backfills fell below the I–D–F curves, suggesting that the RSSs would fail when subjected to the potential regional rainfall.

Although this study examined the hydrological conditions in a specific region (i.e. Taipei) to analyze the performance and design of RSSs subjected to regional rainfall, the proposed methodology can be applied for GRS structures in other regions. The proposed modeling approach and the concept of a rainfall threshold provide a useful method for realistically accounting for regional hydrological conditions and improving the current designs of GRS structures against rainfall. The results and discussion presented in this study are based on the assumption that the drainage system in the RSSs malfunctioned and become ineffective with time, as reported in several failure case studies. This assumption could lead to conservative results compared to the conditions if the drainage system functions properly. In addition, the initial hydrological condition in the ground could vary case by case and differ from the conditions analyzed in this study. Further investigations are required for RSSs with different drainage and ground hydrological conditions. Finally, reliability-based designs that consider the variability and uncertainty of backfill properties and the probability of rainfall conditions are an interesting topic for future research evaluating failure probability and risk level among GRS structures subjected to rainfall.

ACKNOWLEDGMENT

The financial support for this research was from the Ministry of Science and Technology of Taiwan under grant no. MOST107-2628-E-002-003-MY3. The second author would also like to acknowledge the financial support for his Ph.D. study provided by the Taiwan Ministry of Education under the grant for ‘Aim for the Top-Tier University Project’.

NOTATION

Basic SI units are given in parentheses.

a_1, a_2, a_3	constants in Horner's formula (dimensionless)
c	cohesion of saturated soil (Pa)
c'	effective cohesion (Pa)
c'_a	interface cohesion (Pa)
D	total duration of rainfall (s)
E_{inter}	interface efficiency factor (dimensionless)
FS	factor of safety (dimensionless)
H	height of the slope (m)
h	total hydraulic head (m)
h_p	pressure head (m)
I	rainfall intensity (m/s)
I_1	rainfall intensity of initial conditions (m/s)
I_2	rainfall intensity of major rainfall (m/s)
k	unsaturated hydraulic conductivity (m/s)
k_{sat}	saturated hydraulic conductivity (m/s)
L	length of the reinforcement (m)
L_e	horizontal distance to the free end of reinforcement (m)
n	fitting parameter for van Genuchten equations (dimensionless)
P_r	pullout resistance (N/m)
q	input infiltration flux (m/s)
R	accumulated rainfall (m)
R_c	reinforcement coverage ratio (dimensionless)
r_u	porewater pressure coefficient (dimensionless)
S_v	reinforcement vertical spacing (m)
T	reinforcement tensile strength (N/m)
t	time (s)
t_1	duration of initial conditions (s)
t_2	duration of major rainfall (s)
u	porewater pressure at the slope base (Pa)
u_a	pore air pressure (Pa)
u_w	porewater pressure (Pa)
α	fitting parameter for van Genuchten equations (Pa^{-1})
γ	unit weight of the soil (N/m^3)
γ_w	unit weight of water (N/m^3)
δ'	interfacial friction angle ($^\circ$)
θ_r	residual volumetric water content (dimensionless)
θ_s	saturated volumetric water content (dimensionless)
θ_w	volumetric water content (dimensionless)
σ_n	total normal stress (Pa)
σ'_v	overburden pressure on the reinforcement layer (Pa)
τ	soil shear strength (Pa)
ϕ	friction angle ($^\circ$)
ϕ'	effective friction angle ($^\circ$)
ϕ^b	angle indicating the rate of increase in shear strength relative to the matric suction ($^\circ$)
ψ	as-compacted matric suction (Pa)

ABBREVIATIONS

AASHTO	American Association of State Highway and Transportation Official
FC	finer content of soil
FHWA	Federal Highway Administration (USA)
GRS	geosynthetic-reinforced soil
I–D	intensity–duration
I–D–F	intensity–duration–frequency
MSE	mechanically stabilized earth
NCMA	National Concrete Masonry Association
PWP	porewater pressure
RSS	reinforced soil slope
SWCC	soil–water characteristic curve

REFERENCES

- AASHTO (American Association of State Highway and Transportation Officials) (2002). *Standard Specifications for Highway Bridges*, American Association of State Highway and Transportation Officials, Washington, DC, USA.
- Abu-Farsakh, M., Coronel, J. & Tao, M. J. (2007). Effect of soil moisture content and dry density on cohesive soil-geosynthetic interactions using large direct shear tests. *Journal of Material in Civil Engineering*, **19**, No. 7, 540–549.
- Aleotti, P. (2004). A warning system for rainfall-induced shallow failures. *Engineering Geology*, **73**, No. 3–4, 247–265.
- Balakrishnan, S. & Viswanadham, B. V. S. (2016). Performance evaluation of geogrid reinforced soil walls with marginal backfills through centrifuge model tests. *Geotextiles and Geomembranes*, **44**, No. 1, 95–108.
- Berg, R. R. (2010). Fill walls: recent advances and future trends. *Proceeding of the 2010 Earth Retention Conference (ER)*, Richard, F., Hashash, Y. M. A. & Arduino, P., Editors, American Society of Civil Engineers, Reston, VA, USA, pp. 19–36.
- Berg, R., Christopher, B. R. & Samtani, N. (2009). *Design and Construction of Mechanically Stabilized Earth Walls and Reinforced Soil Slopes*, National Highway Institute, Federal Highway Administration, Washington, DC, USA.
- Bhattacharjee, D. & Viswanadham, B. V. S. (2015). Numerical studies on the performance of hybrid-geosynthetic-reinforced soil slopes subjected to rainfall. *Geosynthetics International*, **22**, No. 6, 411–427.
- Blake, J. R., Renaud, J. P., Anderson, M. G. & Hencher, S. R. (2003). Prediction of rainfall-induced transient water pressure head behind a retaining wall using a high-resolution finite element model. *Computers and Geotechnics*, **30**, No. 6, 431–442.
- Caine, N. (1980). The rainfall intensity–duration control of shallow landslides and debris flows. *Geografiska Annaler*, **62**, No. 1–2, 23–27.
- Chen, H. T., Hung, W. Y., Chang, C. C., Chen, Y. J. & Lee, C. J. (2007). Centrifuge modeling test of a geotextile-reinforced wall with a very wet clayey backfill. *Geotextiles and Geomembranes*, **25**, No. 6, 346–359.
- Chen, C. W., Saito, H. & Oguchi, T. (2015). Rainfall intensity–duration conditions for mass movements in Taiwan. *Progress in Earth and Planetary Science*, **2**, No. 1, 14.
- Cheng, K. S., Lin, G. F., Wang, R. Y., Hsu, M. H., Yu, G. H., Yu, P. S. & Lee, K. T. (2001). *Handbook for Hydrological Design*, Water Resources Agency, Ministry of Economic Affairs, Taipei, Taiwan (in Chinese).
- Chinkulkijniwat, A., Yubonchit, S., Horpibulsuk, S., Jothityangkoon, C., Jeetaku, C. & Arulrajah, A. (2016). Hydrological responses and stability analysis of shallow slopes with cohesionless soil subjected to continuous rainfall. *Canadian Geotechnical Journal*, **53**, No. 12, 2001–2013.

- Choudhary, A. K. & Krishna, A. M. (2016). Experimental investigation of interface behaviour of different types of granular soil/geosynthetics. *International Journal of Geosynthetics and Ground Engineering*, **2**, No. 1, 4.
- Duncan, J. M., Wright, S. G. & Brandon, T. L. (2014). *Soil Strength and Slope Stability*, 2nd Edition, John Wiley & Sons, Inc., Hoboken, NJ, USA.
- Eigenbrod, K. D. & Locker, J. G. (1987). Determination of friction values for the design of side slopes lined or protected with geosynthetics. *Canadian Geotechnical Journal*, **24**, No. 4, 509–519.
- Elias, V., Christopher, B. R. & Berg, R. (2001). *Mechanically Stabilized Earth Walls and Reinforced Soil Slopes Design and Construction Guidelines*, National Highway Institute, Federal Highway Administration, Washington, DC, USA.
- Esmaili, D., Hatami, K. & Miller, G. A. (2014). Influence of matric suction on geotextile reinforcement-marginal soil interface strength. *Geotextiles and Geomembranes*, **42**, No. 2, 139–153.
- Fredlund, D. G., Morgenstern, N. R. & Widger, A. (1978). Shear strength of unsaturated soils. *Canadian Geotechnical Journal*, **15**, No. 3, 313–321.
- Garcia, E. F., Gallage, C. P. K. & Uchimura, T. (2007). Function of permeable geosynthetics in unsaturated embankments subjected to rainfall infiltration. *Geosynthetics International*, **14**, No. 2, 89–99.
- Geo-Slope (2012a). *Seep/W for Finite Element Seepage Analysis: User's Guide*, Geo-Slope International Ltd, Calgary, AB, Canada.
- Geo-Slope (2012b). *Slope/W for Slope Stability Analysis: User's Guide*, Geo-Slope International Ltd, Calgary, AB, Canada.
- Guzzetti, F., Peruccacci, S., Rossi, M. & Stark, C. P. (2007). The rainfall intensity–duration control of shallow landslides and debris flows: an update. *Landslides*, **5**, No. 1, 3–17.
- Hong, M., Kim, J. & Jeong, S. (2018). Rainfall intensity–duration thresholds for landslide prediction in South Korea by considering the effects of antecedent rainfall. *Landslides*, **15**, No. 3, 523–534.
- Hossain, M. S., Kibria, G., Khan, M. S., Hossain, J. & Taufiq, T. (2012). Effects of backfill soil on excessive movement of MSE wall. *Journal of Performance of Construction Facilities*, **26**, No. 6, 793–802.
- Iryo, T. & Rowe, R. K. (2005). Infiltration into an embankment reinforced by nonwoven geotextiles. *Canadian Geotechnical Journal*, **42**, No. 4, 1145–1159.
- Karthikeyan, M., Tan, T. S. & Phoon, K. K. (2001). Numerical oscillation in seepage analysis of unsaturated soils. *Canadian Geotechnical Journal*, **38**, No. 3, 639–651.
- Kim, W. S. & Borden, R. H. (2013). Numerical simulation of MSE wall behavior induced by surface-water infiltration. *Journal of Geotechnical and Geoenvironmental Engineering*, **139**, No. 12, 2110–2124.
- Koerner, R. M. & Koerner, G. R. (2013). A data base, statistics and recommendations regarding 171 failed geosynthetic reinforced mechanically stabilized earth (MSE) walls. *Geotextiles and Geomembranes*, **40**, 20–27.
- Koerner, R. M. & Koerner, G. R. (2018). An extended data base and recommendations regarding 320 failed geosynthetic reinforced mechanically stabilized earth (MSE) walls. *Geotextiles and Geomembranes*, **46**, No. 6, 904–912.
- Koutsourais, M., Sandri, D. & Swan, R. (1998). Soil interaction characteristics of geotextiles and geogrids. *Proceedings of the 6th International Conference on Geosynthetics*, Rowe, R. K., Editor, Industrial Fabrics Association International, IFAI, Atlanta, GA, USA, pp. 739–744.
- Leonards, G. A., Frost, J. D. & Bray, J. D. (1994). Collapse of geogrid-reinforced retaining structure. *Journal of Performance of Construction Facilities*, **8**, No. 4, 274–292.
- Liu, C. N., Zornberg, J. G., Chen, T. C., Ho, Y. H. & Lin, B. H. (2009). Behavior of geogrid-sand interface in direct shear mode. *Journal of Geotechnical and Geoenvironmental Engineering*, **135**, No. 12, 1863–1871.
- Liu, C. N., Yang, K. H., Ho, Y. H. & Chang, C. M. (2012). Lessons learned from three failures on a high steep geogrid-reinforced slope. *Geotextiles and Geomembranes*, **34**, 131–143.
- Matsushi, Y. & Matsukura, Y. (2007). Rainfall thresholds for shallow landsliding derived from pressure-head monitoring: cases with permeable and impermeable bedrocks in Boso Peninsula, Japan. *Earth Surface Processes and Landforms*, **32**, No. 9, 1308–1322.
- Mitchell, J. K. & Zornberg, J. G. (1995). Reinforced soil structures with poorly draining backfills part II: case histories and applications. *Geosynthetics International*, **2**, No. 1, 265–307.
- Miyata, Y. & Shinoda, M. (2016). A case study of damages of geogrid reinforced soil walls triggered by rainfall. *Proceedings of the 6th Asian Regional Conference on Geosynthetics: Geosynthetics for Infrastructure Development*, Indian Chapter of International Geosynthetics Society, New Delhi, India, pp. 450–454.
- Miyata, Y., Bathurst, R. J., Konami, T. & Dobashi, K. (2010). Influence of transient flooding on multi-anchor walls. *Soils and Foundations*, **50**, No. 3, 371–382.
- Mualem, Y. (1976). A new model for predicting the hydraulic conductivity of unsaturated porous media. *Water Resources Research*, **12**, No. 3, 593–622.
- Muntohar, A. S., Ikhsan, J. & Liao, H. J. (2013). Influence of rainfall patterns on the instability of slopes. *Civil Engineering Dimension*, **15**, No. 2, 120–128.
- NCMA (National Concrete Masonry Association) (2010). *Design Manual for Segmental Retaining Walls*, National Concrete Masonry Association, Herndon, VA, USA.
- Ng, C. W. W. & Shi, Q. (1998). A numerical investigation of the stability of unsaturated soil slopes subjected to transient seepage. *Computers and Geotechnics*, **22**, No. 1, 1–28.
- Portelinha, F. H. M. & Zornberg, J. G. (2014). Development of capillary barriers during water infiltration in a geotextile-reinforced soil wall. *Proceedings of 10th International Conference of Geosynthetics*, Deutsche Gesellschaft fuer Geotechnik (DGGT), Berlin, Germany, pp. 1–7.
- Portelinha, F. H. M. & Zornberg, J. G. (2017). Effect of infiltration on the performance of an unsaturated geotextile-reinforced soil wall. *Geotextiles and Geomembranes*, **45**, No. 3, 211–226.
- Portelinha, F. H. M., Bueno, B. S. & Zornberg, J. G. (2013). Performance of nonwoven geotextile-reinforced walls under wetting conditions: laboratory and field investigations. *Geosynthetics International*, **20**, No. 2, 90–104.
- Rahardjo, H., Li, X. W., Toll, D. G. & Leong, E. C. (2001). The effect of antecedent rainfall on slope stability. *Geotechnical and Geological Engineering*, **19**, No. 3/4, 371–399.
- Rahardjo, H., Ong, T. H., Rezaur, R. B. & Leong, E. C. (2007). Factors controlling instability of homogeneous soil slopes under rainfall. *Journal of Geotechnical and Geoenvironmental Engineering*, **133**, No. 12, 1532–1543.
- Rahimi, A., Rahardjo, H. & Leong, E. C. (2011). Effect of antecedent rainfall patterns on rainfall-induced slope failure. *Journal of Geotechnical and Geoenvironmental Engineering*, **137**, No. 5, 483–491.
- Raisinghani, D. V. & Viswanadham, B. V. S. (2011). Centrifuge model study on low permeable slope reinforced by hybrid geosynthetics. *Geotextiles and Geomembranes*, **29**, No. 6, 567–580.
- Ran, Q., Hong, Y., Li, W. & Gao, J. (2018). A modelling study of rainfall-induced shallow landslide mechanisms under different rainfall characteristics. *Journal of Hydrology*, **563**, 790–801.
- Rassam, D. W. & Cook, F. (2002). Predicting the shear strength envelope of unsaturated soils. *Geotech Test Journal*, **25**, No. 2, 215–220.
- Robinson, J. D., Vahedifard, F. & AghaKouchak, A. (2016). Rainfall-triggered slope instabilities under a changing climate: comparative study using historical and projected precipitation extremes. *Canadian Geotechnical Journal*, **54**, No. 1, 117–127.
- Saito, H., Nakayama, D. & Matsuyama, H. (2010). Relationship between the initiation of a shallow landslide and rainfall intensity–duration thresholds in Japan. *Geomorphology*, **118**, No. 1–2, 167–175.
- Scarborough, J. A. (2005). A tale of two walls: case histories of failed MSE walls. *Proceedings of Geo-Frontiers 2005*, Gabr, M. A.,

- Bowders, J. J., Elton, D. & Zornberg, J. G., Editors, American Society of Civil Engineers, Reston, VA, USA, pp. 2751–2762.
- Shibuya, S., Kawaguchi, T. & Chae, J. (2007). Failure of reinforced earth as attacked by typhoon No. 23 in 2004. *Soils and Foundation*, **47**, No. 1, 153–160.
- Spencer, E. (1967). A method of analysis of the stability of embankments assuming parallel inter-slice forces. *Géotechnique*, **17**, No. 1, 11–26.
- Suradi, M. & Fourie, A. B. (2014). The effect of rainfall patterns on the mechanisms of shallow slope failure. *ACEH International Journal of Science and Technology*, **3**, No. 1, 1–18.
- Suradi, M., Fourie, A. B. & Saynor, M. J. (2016). An experimental and numerical study of a landslide triggered by an extreme rainfall event in northern Australia. *Landslides*, **13**, No. 5, 1125–1138.
- Tan, T. S., Phoon, K. K. & Chong, P. C. (2004). Numerical study of finite element method based solutions for propagation of wetting fronts in unsaturated soil. *Journal of Geotechnical and Geoenvironmental Engineering*, **130**, No. 3, 254–263.
- Terlien, M. T. J. (1998). The determination of statistical and deterministic hydrological landslide-triggering thresholds. *Environmental Geology*, **35**, No. 2-3, 124–130.
- Thuo, J. N., Yang, K. H. & Huang, C. C. (2015). Infiltration into unsaturated reinforced slopes with nonwoven geotextile drains sandwiched in sand layers. *Geosynthetics International*, **22**, No. 6, 457–474.
- Tsai, T. L. & Wang, J. K. (2011). Examination of influences of rainfall patterns on shallow landslides due to dissipation of matric suction. *Environmental Earth Science*, **63**, No. 1, 65–75.
- Tsaras, I., Rahardjo, H., Toll, D. G. & Leong, E. C. (2002). Controlling parameters for rainfall-induced landslides. *Computers and Geotechnics*, **29**, No. 1, 1–27.
- Vahedifard, F., Mortezaei, K., Leshchinsky, B. A., Leshchinsky, D. & Lu, N. (2016). Role of suction stress on service state behavior of geosynthetic-reinforced soil structures. *Transportation Geotechnics*, **8**, 45–56.
- Vahedifard, F., Tehrani, F. S., Galavi, V., Ragno, E. & AghaKouchak, A. (2017). Resilience of MSE walls with marginal backfill under a changing climate: quantitative assessment for extreme precipitation events. *Journal of Geotechnical and Geoenvironmental Engineering*, **143**, No. 9, 04017056.
- Valentine, R. J. (2013). An assessment of the factors that contribute to the poor performance of geosynthetic-reinforced earth retaining walls. *International Symposium on Design and Practice of Geosynthetic-Reinforced Soil Structures*, Ling, H. I., Editor, DEStech Publications, Inc., Lancaster, PA, USA, pp. 318–327.
- Van, D. B., Chinkulkijniwat, A., Horpibulsuk, S., Yubonchit, S., Limrat, I., Arulrajah, A. & Jothityangkoon, C. (2017). Steady flow in mechanically stabilised earth walls using marginal soils with geocomposites. *Geosynthetics International*, **24**, No. 6, 590–606.
- Vanapalli, S. K., Fredlund, D. G., Pufahl, D. E. & Clifton, A. W. (1996). Model for the prediction of shear strength with respect to soil suction. *Canadian Geotechnical Journal*, **33**, No. 3, 379–392.
- van Genuchten, M. T. (1980). A closed form equation for predicting the hydraulic conductivity of unsaturated soils. *Soil Science Society of America Journal*, **44**, No. 5, 892–898.
- Viswanadham, B. V. S., Razeghi, H. R., Mamaghanian, J. & Manikumar, C. H. S. G. (2017). Centrifuge model study on geogrid reinforced soil walls with marginal backfills with and without chimney sand drain. *Geotextiles and Geomembranes*, **45**, No. 5, 430–446.
- Wu, J. T. H. (2019). *Geosynthetics Reinforced Soil (GRS) Walls*, Wiley-Blackwell, Oxford, UK.
- Wu, J. Y. & Chou, N. N. (2013). Forensic studies of geosynthetic reinforced structure failures. *Journal of Performance of Construction Facilities*, **27**, No. 5, 604–613.
- Wu, J. Y. & Tang, A. H. (2008). Wetting-induced geosynthetic reinforced slope failure. *Proceedings of the 4th Asian Regional Conference on Geosynthetics*, Li, G., Chen, Y. & Tang, X., Editors, Springer, Berlin, Germany, pp. 229–233.
- Yang, K. H., Thuo, J. N., Huynh, V. D. A., Nguyen, T. S. & Portelinha, F. H. M. (2018). Numerical evaluation of reinforced slopes with various backfill-reinforcement-drainage systems subject to rainfall infiltration. *Computers and Geotechnics*, **96**, 25–39.
- Yang, K. H., Thuo, J. N., Chen, J. W. & Liu, C. N. (2019). Failure investigation of a geosynthetic-reinforced soil slope subjected to rainfall. *Geosynthetics International*, **26**, No. 1, 42–65.
- Yoo, C. & Jung, H. Y. (2006). Case history of geosynthetic reinforced segmental retaining wall failure. *Journal of Geotechnical and Geoenvironmental Engineering*, **132**, No. 12, 1538–1548.
- Zapata, C. E., Houston, W. N., Houston, S. L. & Walsh, K. D. (2000). *Soil-Water Characteristic Curve Variability. ASCE Geotechnical Special Publication 99*, American Society of Civil Engineers, Denver, CO, USA.
- Zhang, L. L., Fredlund, D. G., Fredlund, M. D. & Wilson, G. W. (2014). Modeling the unsaturated soil zone in slope stability analysis. *Canadian Geotechnical Journal*, **51**, No. 12, 1384–1398.

The Editor welcomes discussion on all papers published in *Geosynthetics International*. Please email your contribution to discussion@geosynthetics-international.com by 15 April 2020.